Journal of Human Evolution 99 (2016) 52–78

Contents lists available at ScienceDirect

Journal of Human Evolution

journal homepage: www.elsevier.com/locate/jhevol

First virtual endocasts of adapiform primates

Arianna R. Harrington [a, b, c, *], Mary T. Silcox [d], Gabriel S. Yapuncich [c], Doug M. Boyer [c, e], Jonathan I. Bloch [a]

[a] Florida Museum of Natural History, University of Florida, Gainesville, FL 32611, USA
[b] Department of Biology, University of Florida, Gainesville, FL 32611, USA
[c] Department of Evolutionary Anthropology, Duke University, Durham, NC 27708, USA
[d] Department of Anthropology, University of Toronto, Scarborough, Toronto, Ontario M1C 1A4, Canada
[e] New York Consortium in Evolutionary Primatology (NYCEP), American Museum of Natural History, New York, NY 10024, USA

ARTICLE INFO

Article history:
Received 23 December 2015
Accepted 30 June 2016

Keywords:
Endocast
Primate
Adapiforms
Brain evolution
Eocene
North America

ABSTRACT

Well-preserved crania of notharctine adapiforms from the Eocene of North America provide the best direct evidence available for inferring neuroanatomy and encephalization in early euprimates (crown primates). Virtual endocasts of the notharctines *Notharctus tenebrosus* ($n = 3$) and *Smilodectes gracilis* ($n = 4$) from the middle Eocene Bridger formation of Wyoming, and the late Eocene European adapid adapiform *Adapis parisiensis* ($n = 1$), were reconstructed from high-resolution X-ray computed tomography (CT) data. While the three species share many neuroanatomical similarities differentiating them from plesiadapiforms (stem primates) and extant euprimates, our sample of *N. tenebrosus* displays more variation than that of *S. gracilis*, possibly related to differences in the patterns of cranial sexual dimorphism or within-lineage evolution. Body masses predicted from associated teeth suggest that *N. tenebrosus* was larger and had a lower encephalization quotient (EQ) than *S. gracilis*, despite their close relationship and similar inferred ecologies. Meanwhile, body masses predicted from cranial length of the same specimens suggest that the two species were more similar, with overlapping body mass and EQ, although *S. gracilis* exhibits a range of EQs shifted upwards relative to that of *N. tenebrosus*. While associated data from other parts of the skeleton are mostly lacking for specimens included in this study, measurements for unassociated postcrania attributed to these species yield body mass and EQ estimates that are also more similar to each other than those based on teeth. Regardless of the body mass prediction method used, results suggest that the average EQ of adapiforms was similar to that of plesiadapiforms, only overlapped the lower quadrant for the range of extant strepsirrhines, and did not overlap with the range of extant haplorhines. However, structural changes evident in these endocasts suggest that early euprimates relied more on vision than olfaction relative to plesiadapiforms, despite having relatively small endocranial volumes compared to extant taxa.

© 2016 Elsevier Ltd. All rights reserved.

1. Introduction

Compared to many other mammal groups, on average the brains of extant primates are large when controlling for body mass (Martin, 1990; Barton, 2006). This is often cited as a potentially diagnostic characteristic of the order Primates (e.g., Cartmill, 1992) and various studies have correlated differences in relative brain size within and outside of Primates with ecological and social variables in attempts to understand the selective pressures that drove the evolution of increased relative brain size in this lineage (e.g., Clutton-Brock and Harvey, 1980; Dunbar, 1998; Healy and Rowe, 2007). Despite the potential importance of this characteristic to understanding primate evolution, the pattern and timing of brain evolution in the earliest fossil euprimates (crown primates) is not well understood. In particular, whether or not brain morphology and relative encephalization of early fossil crown primates differed in significant ways relative to that of stem primates ("plesiadapiforms") is poorly documented. Yet such information is critical for understanding the unifying features of the primate clade and the ecological context of primate origins.

Although soft tissues of internal organs do not typically fossilize, endocranial endocasts, or the casts of the internal cranial cavity

* Corresponding author.
E-mail address: arianna.harrington@duke.edu (A.R. Harrington).

http://dx.doi.org/10.1016/j.jhevol.2016.06.005
0047-2484/© 2016 Elsevier Ltd. All rights reserved.

(Jerison, 1973), are one way in which relative brain size and morphology of extinct mammals may be studied. Because the brains of mammals occupy much of the volume of the internal cranial cavity, mammalian endocasts provide a relatively accurate proxy for brain size and external morphology, particularly for small mammals (Jerison, 1973; Macrini, 2007). This paper describes a sample of virtual endocasts of three Eocene adapiform primates, *Notharctus tenebrosus*, *Smilodectes gracilis*, and *Adapis parisiensis*, to assess ontogenetic, temporal, and sexual signals in endocast morphology and to re-evaluate the hypothesis that the earliest crown primates were more encephalized and/or differed in endocranial morphology relative to stem primates.

Crown primates (sometimes also referred to as "primates of modern aspect"; Simons, 1972, Wible and Covert, 1987; but see Boyer et al., 2013b, p. 39 for reasons to avoid this term), include all extant primates and their extinct direct relatives (Hoffstetter, 1977; Szalay and Delson, 1979; Martin, 1990). 'Euprimates' is a specific formulation of crown primates that includes Eocene adapiforms as stem strepsirrhines and omomyiforms as stem haplorhines (Hoffstetter, 1977). Plesiadapiformes is a paraphyletic group of Paleogene stem primates that includes the superfamily Plesiadapoidea, suggested to be the sister group of Euprimates (Bloch et al., 2007). Omomyiformes (also known as Omomyoidea) and Adapiformes (also known as Adapoidea) are two clades of early euprimates that had diverged by the earliest Eocene (Rose, 1994). While omomyiforms are recognized from the earliest Eocene to early Miocene of Asia, Europe, and North America, adapiforms are recognized from the earliest Eocene to late Miocene of Europe, Africa, and Asia (Gebo, 2002; Gunnell and Rose, 2002; Rasmussen, 2007). Adapiformes is typically divided into six families: the Eocene European family Adapidae, the Eocene Asian family Asiadapidae, the Eocene European, African, and Asian family Caenopithecidae, the Eocene through Miocene Asian family Sivaladapidae, the Eocene Asian and European family Cercamoniidae, and the Eocene European and predominantly North American family Notharctidae (Fleagle, 2013). The phylogenetic relationships of adapiforms have long been debated, with suggested affinities to either haplorhines (e.g., Gingerich, 1980; Rasmussen, 1987; Franzen et al., 2009; Gingerich et al., 2010) or to lemuroids, prosimians, or strepsirrhines (Gregory, 1920; Beard et al., 1986; Martin, 1990), with similarities to haplorhines (see Kay et al., 1997; Maiolino et al., 2012) explained as the result of convergent evolution (Seiffert et al., 2009). In the latter phylogenetic context, adapiforms are classified as stem strepsirrhines (Williams et al., 2010a,b; Maiolino et al., 2012), while omomyiforms are classified as stem haplorhines (Williams et al., 2010b).

Within Primates, endocasts of both plesiadapiforms and euprimates are known. These include endocasts produced by natural sediment infillings of the endocranium (e.g., Gazin, 1965), from artificially derived representations of the inner surface made of materials such as latex (e.g., Gingerich and Martin, 1981), and by virtual segmentation of sequential images produced by high-resolution X-ray micro computed tomography (CT) scanning (e.g., Silcox et al., 2009b, 2010; Kirk et al., 2014; Orliac et al., 2014; Ramdarshan and Orliac, 2015). Published plesiadapiform, adapiform, and omomyiform endocasts are summarized in Table 1.

These endocasts have formed the basis of understanding encephalization and endocranial morphology in stem primates and early euprimates and are often discussed in a comparative context (e.g., Radinsky, 1970; Gurche, 1978; Martin, 1990; Silcox et al., 2010), but the different endocast reconstruction methods pose some comparative limitations. Primate endocasts described and analyzed prior to Silcox et al. (2009b) – which include both natural and artificial physical endocasts (or a composite of both) of varying degrees of completeness (e.g., Gazin, 1965; Gingerich and Martin, 1981) – may have obscured morphology due to preservation of overlying bone (e.g., Hofer and Wilson, 1967; Radinsky, 1967; Gurche, 1982), and/or poorer surface resolution compared to virtual endocasts (e.g., Silcox et al., 2009b, 2010; Kirk et al., 2014; Orliac et al., 2014; Ramdarshan and Orliac, 2015). In addition, because of the difficulties in obtaining high quality endocasts from well-preserved skulls, sample sizes for fossil euprimate endocasts have been relatively small.

Recent advances in imaging technology have significantly changed the study of primate endocasts. Virtual endocasts of *Ignacius graybullianus* (Silcox et al., 2009b), *Microsyops annectens* (Silcox et al., 2010), *Rooneyia viejaensis* (Kirk et al., 2014), *Plesiadapis tricuspidens* (Orliac et al., 2014), and *Microchoerus erinaceus* (Ramdarshan and Orliac, 2015) have clearly shown that X-ray CT technology presents an unprecedented opportunity to visualize more complete endocasts of specimens where it would have been previously difficult or impossible without damage to the specimen. Virtual endocast reconstruction also allows for more consistent quantitative comparisons, as volumes and other metrics may be measured precisely using the same 3D imaging software. This is important because past studies on natural and artificial endocasts have utilized disparate methods of volume estimation. In the absence of complete endocasts, brain volumes have been estimated mathematically through double graphic integration (Jerison, 1973; Gingerich, 1976; Radinsky, 1977), infilling of cranial space by mustard seeds (Gingerich and Martin, 1981), or by water displacement of partially artistically reconstructed endocasts (Gurche, 1978, 1982).

Since Jerison's (1973) introduction of the encephalization quotient (or EQ, a comparative ratio of the measured brain size of a mammal to the expected brain size of an average mammal of the equivalent body mass) it has been clear that comparison of brain size in fossils requires both the estimation of endocranial volume and the prediction of body mass. An additional source of variation among

Table 1
Published endocasts of plesiadapiforms and early Euprimates

Taxon	Sources
Megadelphus lundeliusi (Microsyopidae, Plesiadapiformes)	Szalay, 1969; Radinsky, 1977
Microsyops annectens (Microsyopidae, Plesiadapiformes)	Szalay, 1969; Radinsky, 1977; Silcox et al., 2010
Plesiadapis cookei (Plesiadapidae, Plesiadapiformes)	Gingerich and Gunnell, 2005; Orliac et al., 2014
Plesiadapis tricuspidens (Plesiadapidae, Plesiadapiformes)	Orliac et al., 2014
Ignacius graybullianus (Paromomyidae, Plesiadapiformes)	Silcox et al., 2009b
Adapis parisiensis (Adapinae, Adapidae, Adapiformes)	Neumayer, 1906; Gregory, 1920; Le Gros Clark, 1945; Radinsky, 1970; Gurche, 1978, 1982; Gingerich and Martin, 1981; Martin, 1990
Smilodectes gracilis (Notharctinae, Notharctidae, Adapiformes)	Gazin 1965; Radinsky, 1970; Gurche, 1978, 1982; Martin, 1990
Notharctus tenebrosus (Notharctinae, Notharctidae, Adapiformes)	Gregory, 1920; Gurche, 1978, 1982
Tetonius homunculus (Anaptomorphinae, Omomyidae, Omomyiformes)	Radinsky, 1967; Radinsky, 1970; Gurche 1978, 1982
Necrolemur antiquus (Microchoeridae; Omomyiformes)	Hürzeler, 1948; Hofer, 1962; Radinsky, 1970; Gurche, 1978, 1982
Microchoerus erinaceus (Microchoeridae, Omomyiformes)	Ramdarshan and Orliac, 2015
Rooneyia viejaensis (in certae sedis)	Hofer and Wilson, 1967; Radinsky, 1970; Gurche, 1978, 1982; Kirk et al., 2014

studies rests in approaches to predicting body mass. Several early studies of relative encephalization of primates calculated EQ using body mass derived from rough comparisons of the size of fossil primate skeletons to those of extant primates to arrive at an value (Jerison, 1973; Radinsky, 1977; Gurche, 1978, 1982). More recent analyses (Martin, 1990; Gingerich and Gunnell, 2005; Silcox et al., 2009a, 2010; Orliac et al., 2014; Kirk et al., 2014) have used body mass predictions derived from regression analyses that correlated body mass to various measurements of the cranium and postcranial skeleton. These body mass prediction equations were generated using measurements of the teeth (Gingerich et al., 1982; Conroy, 1987; Dagosto and Terranova, 1992), long bones (Gingerich, 1990), crania (Martin, 1990; Silcox et al., 2009a), and tarsals (Dagosto and Terranova, 1992; Boyer et al., 2013a; Yapuncich et al., 2015).

Despite methodological disparities between studies and the resulting complications for comparing data from different publications, a number of researchers have attempted to compile estimates of volumes for the whole brain, olfactory bulbs, and calculations of EQ from natural and artificial endocasts into synthetic treatments of primate olfactory evolution (e.g., Takai et al., 2003; Heritage, 2014) and brain evolution (e.g., Silcox et al., 2009b, 2010; Montgomery et al., 2010; Steiper and Seiffert, 2012). However, it is clear that past studies of early primate encephalization suffer from small sample sizes and lack of comparability in the methods for data collection. In addition, while the record of fossil primate endocasts is growing, virtual endocasts have not been reconstructed for most of the earliest euprimates (Ramdarshan and Orliac, 2015), and are hitherto absent for adapiforms (except for an illustration of a surface laser scan of an undescribed endocast of *A. parisiensis*, FMNH 59259; Jerison, 2007, 2012). This study documents a sample of virtual endocasts of notharctine primates, as well as a new virtual endocast of an adapine primate, in order to begin to rectify this situation.

1.1. Description of taxa in this study

Adapis parisiensis is a late Eocene European adapiform in the family Adapidae. *Notharctus tenebrosus* and *S. gracilis* are North American adapiforms of the family Notharctidae and subfamily Notharctinae. The genus *Notharctus* ranges from the late Wasatchian (equivalent to the Wa7 or Lostcabinian) to the early Uintan (Ui1; Uinta; Shoshonian) North American Land Mammal Ages (NALMA; Gunnell, 1995, 2002; Gunnell et al., 2008, 2009; see Fig. 1). This corresponds to the late early Eocene to middle Eocene epoch, approximately 52.4 Ma–45.7 Ma. The genus *Smilodectes* is present from the early Bridgerian (Br1; Bridger A; Gardnerbuttian) to the late Bridgerian (Br3; Bridger C; Twinbuttean), corresponding to the early- to mid-Middle Eocene epoch, approximately 51 Ma–46.3 Ma (Robinson et al., 2004; Gunnell et al., 2008). *Notharctus* and *Smilodectes* are sometimes hypothesized to be sister taxa that evolved from the earlier notharctid genus *Cantius* (Covert, 1990), while others hypothesize a sister–taxon relationship of *Smilodectes* and another notharctine genus, *Copelemur*, with *Notharctus* grouping closer to a paraphyletic *Cantius* (Beard, 1988; Gunnell, 2002).

Well-preserved fossils of *Notharctus* and *Smilodectes* (e.g., Gregory, 1920; Gazin, 1958; Hamrick and Alexander, 1996; Alexander and Burger, 2001; Maiolino et al., 2012; Boyer et al., 2013b) are best known from the middle Bridgerian biochron (equivalent to Br2, Bridger B, and the upper Blackforkian; Gunnell, 1998, 2002; Gunnell et al., 2008) with an absolute date of 47.96 ± 0.13 Ma from the Church Butte Tuff (Murphey et al., 1999). In particular, *N. tenebrosus* and *S. gracilis* have a well-sampled fossil record including several nearly complete skulls and skeletons (Martin, 1990; Gunnell, 2002). *Notharctus tenebrosus* and *S. gracilis* were contemporaneous and their fossils are found in middle Bridgerian deposits in the Black Forks Member of the Bridger formation in the Green River Basin of Wyoming (Gunnell et al., 2008).

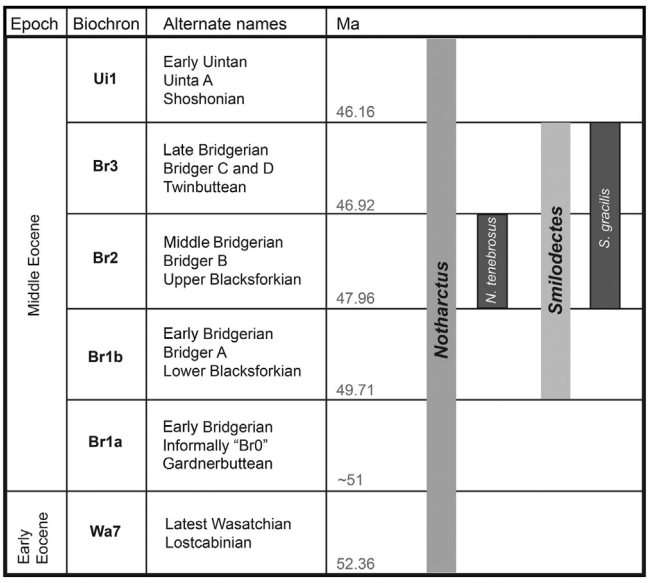

Figure 1. Time periods in which the genera *Notharctus* and *Smilodectes* were present in North America. Data from Gunnell (1995, 1998, 2002), Clyde et al. (1997, 2001); Murphey et al. (1999); Robinson et al. (2004), and Gunnell et al. (2008, 2009).

Natural endocasts of *S. gracilis* are relatively well studied compared to those of *N. tenebrosus*. First figured and described in detail by Gazin (1965), data further elaborating on the endocasts of this species have appeared in Radinsky (1970), Gingerich and Martin (1981), and Gurche (1978, 1982). These publications documented several natural endocasts including those of YPM 12152 and USNM 23276, adding much to the knowledge of the neuroanatomy of *S. gracilis*. However, due to incomplete preservation (USNM 23276) and incomplete preparation (YPM 12152), questions remain about the anatomy and volume of important features, most notably of the olfactory bulbs (Radinsky, 1970).

In contrast, partial endocasts of *Notharctus* were described, but not figured, by Gregory (1920), based on incomplete natural endocasts and observation of the intracranial surface of the skulls of AMNH 11478, AMNH 14656, AMNH 12569, and AMNH 13030 (now recognized as *S. gracilis*). Gurche (1978) expanded on Gregory's work with description of "Endocast A" (an incomplete natural endocast "of uncertain catalog number"; p. 42), casts of petrosal bones of AMNH 12585, AMNH 12575, AMNH 12581, AMNH 12569, and YPM 12958, and olfactory bulb casts of USNM 244365 and another specimen of unknown catalog number ("Endocast B"). Gurche (1978) also described the olfactory bulb morphology of USNM V 23278 from an X-ray in the dorsoventral aspect. While these descriptions somewhat increased understanding of the endocast morphology of *Notharctus*, the specimens were incomplete with many important aspects still not documented.

There were also some methodological complexities with the historical estimations of endocast volume and prediction of body mass (and thus relative encephalization) for *N. tenebrosus* and *S. gracilis*. The most frequently cited endocranial volumes for both *N. tenebrosus* (Gurche, 1982; Martin, 1990) and *S. gracilis* are based on partially artistically restored specimens (Gurche, 1978) or double graphic integration (Radinsky, 1977; Jerison, 1979). Because these authors believed *N. tenebrosus* and *S. gracilis* to be of similar body mass, and brain volume estimates were similar values, the two species' EQs have been reported to be similar (Gurche, 1982).

Whether there are differences in the level of encephalization of *N. tenebrosus* and *S. gracilis* has not been seriously reassessed. This is an interesting question as these two species are relatively closely related phylogenetically, are contemporaries, and are thought to have shared similar diets (Covert, 1986, 1995; Gilbert, 2005; Sauther and Cuozzo, 2012; Fleagle, 2013) and activity patterns (e.g., Sauther and Cuozzo, 2012). Any potential differences in relative encephalization might imply ecological or behavioral differences between the species. The current study also assesses the presence or absence of morphological differences between the endocasts in *S. gracilis* and *N. tenebrosus*.

2. Institutional abbreviations

AMNH, American Museum of Natural History, New York, NY, USA; FMNH, Field Museum of Natural History, Chicago, IL, USA; ISEM, Institut des Sciences de l'Evolution de Montpellier, Montpellier, France; NHM, Natural History Museum, London, United Kingdom; MPM, Milwaukee Public Museum, Milwaukee, Wisconsin, USA; UM, University of Michigan Museum of Paleontology, Ann Arbor, Michigan, USA; USNM, United States National Museum (Smithsonian Institution), Washington, DC, USA; UCM, University of Colorado Museum of Natural History, Boulder, CO, USA; YPM, Yale Peabody Museum, New Haven, CT, USA; VI, Private collection of Mr. Dominique Vidalenc.

3. Materials and methods

3.1. Description of specimens

Virtual endocasts of a total of eight specimens were reconstructed in this study: three *N. tenebrosus* (AMNH 127167, USNM V 23277, and USNM V 23278), four *S. gracilis* (UM 32773 (=MPM 2612), USNM V 17994, USNM V 17996, and USNM V 21815), and one *A. parisiensis* (NHM M 1345). Three-dimensional surface files and original tiff stacks of these crania and 3D surface files of the extracted endocasts are available for download at morphosource.org (Boyer et al., in press). Each specimen used for this study is briefly described below, and the locality, biochron, and a list of associated postcrania are presented in Table 2.

AMNH 127167 (http://dx.doi.org/10.17602/M2/M10905) is a partial skeleton of an adult (M_3 erupted) *N. tenebrosus*. The cranium of this specimen (Supplementary Online Material [SOM] Fig. 1A, B) is somewhat dorsoventrally compressed and is slightly distorted. The lateral margin of the right supraorbital process is displaced caudally in the coronal plane relative to the left supraorbital process, and the right maxilla is compressed in the sagittal plane when compared to the left maxilla. Both supraorbital processes and the right maxilla bear puncture marks that may have been inflicted by an avian predator (Alexander and Burger, 2001). Relatively large canines and flared zygomatics led to the interpretation that AMNH 127167 is a male (Alexander, 1994; Alexander and Burger, 2001). Cranial and postcranial morphology of AMNH 127167 has been documented in several previous studies (Hamrick and Alexander, 1996; Alexander and Burger, 2001; Silcox et al., 2009a; O'Leary et al., 2013; Boyer et al., 2013b).

USNM V 23277 (http://dx.doi.org/10.17602/M2/M10957) is a skull of an adult *N. tenebrosus* (SOM Fig. 1C, D). The cranium is largely complete, missing only portions of the right postorbital bar, zygomatic arch, right canine, and premaxilla. While the left zygomatic arch shows some lateral crushing, the braincase is relatively undistorted, with no evidence of breakage along the dorsal or lateral surface of the neurocranium.

USNM V 23278 (http://dx.doi.org/10.17602/M2/M10958) is a skull of *N. tenebrosus* (SOM Fig. 1E, F). This cranium shows more

Table 2
Summary of specimens in this sample.

Specimen	Species	Sex assignment	Locality	Biochron	Associated postcrania	DOI to endocast on morphosource.org
AMNH 127167	*N. tenebrosus*	Male	Butch Hill, north side of Grizzly Buttes (Uinta County, WY)	Br2	Cervical, thoracic, lumbar vertebrae, distal right and left femora, left and right proximal tibiae, incomplete fibula, right and left humeri, an ulna, left radius, nearly complete left hand	http://dx.doi.org/10.17602/M2/M10905
USNM V 23277	*N. tenebrosus*	Female	10 mi east of Lyman (Uinta County, WY)	Br2	None	http://dx.doi.org/10.17602/M2/M10957
USNM V 23278	*N. tenebrosus*	Female	0.5 miles south of Church Buttes (Uinta County, WY)	Br2	None	http://dx.doi.org/10.17602/M2/M10958
UM 32773 (=MPM 2612)	*S. gracilis*	n/a	UM locality BRW-15 (Sweetwater County, WY)	Br2	None	http://dx.doi.org/10.17602/M2/M11008
USNM V 17994	*S. gracilis*	Male	Northern part of Twin Buttes (Sweetwater County, WY)	Br3	Portions of the axial and appendicular skeleton, including left astragalus	http://dx.doi.org/10.17602/M2/M11006
USNM V 17996	*S. gracilis*	Female	Pinnacle Rock (Sweetwater County, WY)	Br3	None	http://dx.doi.org/10.17602/M2/M10959
USNM V 21815	*S. gracilis*	Female	Church Buttes (Uinta County, WY)	Br2	Portions of the axial and appendicular skeleton	http://dx.doi.org/10.17602/M2/M10960
NHM M 1345	*A. parisiensis*	Male	Caylux, Tarn-et-Garonne, France	Headonian (European land mammal age)	None	http://dx.doi.org/10.17602/M2/M11050

damage than the other two *N. tenebrosus* specimens included in this study. While the specimen shows minimal dorsoventral or lateral compression, it exhibits bilateral damage to the orbital and zygomatic regions and further damage to the occipital, squamosal, petrosal, palatine, and maxillary regions. The specimen is an adult with all preserved teeth erupted, yet many teeth are either missing or damaged, including the right tooth row rostral to P^3 and the left tooth row rostral to M^1. Assessing an X-ray image of USNM V 23278, Gurche observed that the olfactory bulbs were likely "widely diverging" (1978: p. 48).

USNM V 17994 (http://dx.doi.org/10.17602/M2/M11006), USNM V 21815 (http://dx.doi.org/10.17602/M2/M10960), and USNM V 17996 (http://dx.doi.org/10.17602/M2/M10959) are hypotype specimens of adult *S. gracilis* figured by Gazin (1958). USNM V 17994 (SOM Fig. 1I, J) consists of a nearly complete adult cranium missing only fragments of the right bulla, premaxilla, and I^1–P^1. The cranium is minimally distorted, exhibiting little sign of dorsoventral crushing and only a slight lateral shift of the orbits to the left. USNM V 21815 is a partial skeleton of an adult *S. gracilis*. The cranium (SOM Fig. 1K, L) and dentaries of this specimen are fairly complete. In addition to retaining the neurocranium, orbits, zygomatic arches, and much of the maxillae with teeth, this specimen preserves much of the premaxilla (although the incisors are missing). Compared to USNM V 17994, the cranium of USNM V 21815 is less flared in the zygomatic region. The neurocranium of USNM V 21815 appears to be dented on the left side around the temporal region at the junction of the temporal and parietal bones, although the cross-sectional view of the CT scan does not show a clear break in the bone of the anomalous area. While this feature may be due to plastic deformation during fossilization, it is also possible that this damage occurred during the course of the animal's life and was not a taphonomic effect. USNM V 17996 is not as well-preserved as the other *S. gracilis* specimens, consisting of a distorted adult cranium (SOM Fig. 1M, N) and incomplete mandibles. While the cranial vault is mostly complete and appears undistorted, the rostral portion of this specimen is shifted left and is missing many parts, mainly from the orbital region, nasals, frontals, premaxilla, and maxilla anterior to P^3 on both sides.

UM 32773 (=MPM 2612; http://dx.doi.org/10.17602/M2/M11008) is an incomplete cranium and right dentary of a juvenile *S. gracilis* (SOM Fig. 1O, P) that preserves a fairly complete neurocranium and basicranium although the bullae are broken. Portions of the frontals, squamosals, jugals, nasals, and premaxilla are missing, and the orbital region is poorly preserved. The right maxilla is better preserved than the left. The subadult status of UM 32773 is indicated by the mostly erupted M^3, partially erupted P^2, P^3, and P^4 in the crypt underneath the dP^3 and dP^4, and the canine in the crypt that may be observed in the right maxilla in CT scans (Fig. 2). The right dentary preserves dP_3 and dP_4, erupting incisors and P_2, and fully erupted M_1, M_2, and M_3. The presence of the first molars indicates that the specimen was likely weaned (Smith, 1991). Many sutures in the cranial vault are unfused, including the metopic, coronal, sagittal, and parietal–interparietal sutures. While many bones are missing, there are no signs of dorso-ventral crushing or lateral distortion. This specimen has also been discussed in a number of studies (e.g., Rose et al., 1999; Silcox et al., 2009a).

Finally, NHM M 1345 (http://dx.doi.org/10.17602/M2/M11050; SOM Fig. 1G, H) is a specimen of an adult *A. parisiensis* consisting of a nearly complete cranium missing only the premaxilla and portions of the left jugal and squamosal. An artificial endocast produced from the endocranium of NHM M 1345 has the catalog number NHM M 20192 and has been detailed in other studies (Le Gros Clark, 1945; Gurche, 1978, 1982). Some distortions in this endocast have been noted, primarily dorsoventral crushing in the frontal bone that may have caused flattening of the frontal lobe region in the artificial endocast (Le Gros Clark, 1945; Gingerich and Martin, 1981).

3.2. Developmental stage of UM 32733

To assess the likely age, percent total adult weight and percent total brain mass achieved at the time of death of UM 32773, the juvenile *S. gracilis*, the tooth eruption sequence inferred from the specimen was compared to that of living primates (Tattersall and Schwartz, 1974; Schwartz, 1975; Smith et al., 1994) and approximate age at tooth eruption was estimated by comparison to data from *Saimiri sciureus* (Long and Cooper, 1968; Manocha, 1979; Franzen et al., 2009).

Saimiri sciureus was chosen as a comparative model to understand the age, body mass, and brain mass at the time of death of a juvenile specimen of the cercamoniine adapiform *Darwinius masillae* (PMO 214.214 and WDC-MG-210) relative to the individual's adult brain and body mass as given by Franzen et al. (2009). They proposed the appropriateness of this model due to the relatively fast growth of *S. sciureus*, which is more similar to the primitive growth pattern of non-anthropoids (*Lemur*, *Varecia*, *Eulemur*, *Loris*, *Galago*, and *Tarsius*), in addition to the fact that there

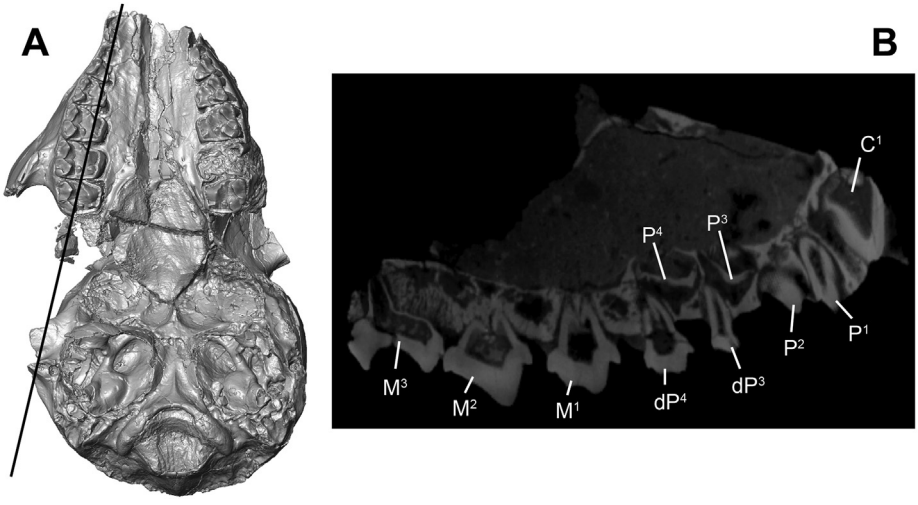

Figure 2. A) Occlusal view of the cranium of the juvenile *Smilodectes gracilis* UM 32773 and B) a CT cross-sectional view of the maxilla. The line denotes the plane of the cross-sectional view.

are data available of an ontogenetic sequence of brain mass and body mass and age at tooth eruption for *S. sciureus*. López Torres et al. (2015) recently re-evaluated the appropriateness of the *S. sciureus* model using an ancestral state reconstruction of the dental eruption pattern in Primates. They argued that a living strepsirrhine model might be better for modeling growth in *D. masillae*, specifically *Eulemur fulvus*, *Eulemur rufus*, and *Varecia variegata*, in light of the similarities in their molar and premolar eruption sequences.

While the eruption sequence for *S. gracilis* is unknown, if the eruption pattern was similar to that of *Notharctus* (Gregory, 1920; Gingerich and Smith, 2010; López Torres et al., 2015), then the most likely postcanine eruption sequence of *S. gracilis* is $M\frac{1}{1}-P\frac{1}{1}-M\frac{2}{2}-M\frac{3}{3}-P\frac{2}{2}-P\frac{4}{4}-P\frac{3}{3}$, which is consistent with the teeth preserved in UM 32773. No modern primate is known with this exact eruption sequence, although it is perhaps most comparable to that of *Eulemur mongoz* ($M\frac{1}{1}-I\frac{2}{2}-I\frac{3}{3}-C_1-M\frac{2}{2}-M\frac{3}{3}-P\frac{2}{2}-C^1-P\frac{4}{4}-P\frac{3}{3}$; Tattersall and Schwartz, 1974), *Otolemur crassicaudatus* $\left(M\frac{1}{1}-I\frac{2}{2}-I\frac{3}{3}-C_1-M\frac{2}{2}-M\frac{3}{3}-P\frac{2}{2}-C^1-P\frac{4}{4}-P\frac{3}{3}\right)$, *Galago gallarum* $\left(M\frac{1}{1}-I\frac{2}{2}-I\frac{3}{3}-C_1-M\frac{2}{2}-M\frac{3}{3}-P\frac{2}{2}-C^1-P\frac{4}{4}-P\frac{3}{3}\right)$, and *Galagoides demidoff* ($M\frac{1}{1}-M\frac{2}{2}-I\frac{2}{2}-I\frac{3}{3}-C_1-M\frac{3}{3}-C^1-P\frac{2}{2}-P\frac{4}{4}-P\frac{3}{3}$; Schwartz, 1975), suggesting that, as for *D. masillae*, a strepsirrhine model may be preferable for *S. gracilis* than one based on *S. sciureus*. Unfortunately, the data necessary to use a strepsirrhine model for age estimation using the methods from Franzen et al. (2009) and López Torres et al. (2015) is incomplete. While there are data relating weight to age of individuals of *E. mongoz* available in the Duke Lemur Center database, there are no data available to relate brain mass or tooth eruption sequence to age for these species. For this reason, we use a *S. sciureus* model to consider the age and degree of development of the brain for *S. gracilis*.

3.3. Sex of specimens

NHM M 1345 (*A. parisiensis*) was previously assessed as a male based on canine size, bizygomatic width, and relative robustness of the sagittal and nuchal crests (Gingerich, 1981). While AMNH 127167 (*N. tenebrosus*) and USNM V 17994 (*S. gracilis*) have both been suggested to be adult males and USNM V 21815 (*S. gracilis*) has been suggested to be an adult female (Alexander, 1994; Alexander and Burger, 2001), the sexes of the other specimens in this sample have not been assessed. For USNM V 23277, USNM V 23278, USNM V 17996, and UM 32773, the length and width of canine roots were measured (Table 3) and craniofacial characters were assessed following the criteria in Alexander (1994). AMNH 127167, USNM V 17994, and USNM V 21815 were reassessed for comparison (see Table 3). Canine root dimensions were compared to those reported in Alexander (1994). All measurements were made with the 2D measurement tool in Avizo 8.1.1 (Visualization Sciences Group, 2007–2015).

3.4. Endocast preparation

For this study, the cranium of each specimen was scanned using high-resolution X-ray computed tomography (μCT). AMNH 127167 was scanned using the OMNI-X Industrial Scanner at the Center of Quantitative Imaging (CQI) at Pennsylvania State University. UM 32773 was scanned using the Nikon XTH 225 ST scanner at the Nikon Metris X-Tek Metrology Systems, Ltd. Headquarters in Brighton, MI. The other six specimens were scanned using the Nikon XTH 225 ST μCT scanner at the Shared Materials Instrumentation Facility (SMIF) at Duke University. The scanning parameters used for each specimen are recorded in SOM Table 1 (with more details available on morphosource.org).

Virtual endocasts of AMNH 127167, UM 32773, USNM V 17994, and NHM M 1345 were manually segmented in ImageJ (Rasband, 1997–2014) from the tiff stacks of the CT datasets. Linear and volumetric measurements were taken following protocols described by Silcox et al. (2010) using the three-dimensional visualization programs Avizo 6.6-8.1.1. USNM V 23277, USNM V 23278, USNM V 17996, and USNM V 21815 were segmented in Avizo 8.1.1 using the magic wand and lasso tools to create a new labelfield in the segmentation editor, but their processing otherwise followed the same protocols as the others. The resulting endocasts and measurements were compared to each other and to published data for extant strepsirrhines, extant haplorhines, and other fossil primates (Radinsky, 1974; Gurche, 1982; Martin, 1990; Isler et al., 2008; Silcox et al., 2009b, 2010; Kirk et al., 2014; Orliac et al., 2014; Ramdarshan and Orliac, 2015).

3.5. Encephalization quotients (EQs)

All EQs were calculated using equations from Jerison (1973) and Eisenberg (1981). Jerison's equation is $EQ = E/(0.12W^{0.67})$ and Eisenberg's equation is $EQ = E/(0.055W^{0.74})$, where EQ = encephalization quotient, E = brain volume, and W = body mass. Martin (1990) has suggested that Jerison's equation tends to yield inaccurate EQ estimates for very small or very large mammals based on his sample, which yields a slope close to that included in Eisenberg's equation. We calculated EQ using both methods in order to make our results comparable with those of a variety of previous studies.

3.6. Neocortical ratios

To calculate neocortical ratios, the surface area of the entire endocast (without the casts of the postglenoid vein and

Table 3
Dental measurements of specimens in the sample.

Specimen	Species	Sex	CL	CW	CH	M^1L	M^1W	M_1L	M_1W
AMNH 127167	*N. tenebrosus*	M	4.29	3.11	8.34	5.58	6.15	5.33	3.97
USNM V 23277	*N. tenebrosus*	F	3.49	2.64	–	5.56	6.57	5.37	4.12
USNM V 23278	*N. tenebrosus*	F	3.55	2.42	–	5.08	6.11	5.73	4.07
USNM V 17994	*S. gracilis*	M	3.62	2.30	–	4.40	5.32	–	–
USNM V 17996	*S. gracilis*	F	–	–	–	4.19	5.40	4.24	3.33
USNM V 21815	*S. gracilis*	F	3.26	2.30	5.12	4.23	5.23	4.87	3.41
UM 32773	*S. gracilis*	?	–	–	–	4.64	5.34	4.55	3.26
NHM M 1345	*A. parisiensis*	M	–	–	–	4.38	4.50	–	–

CL = canine root length; CW = canine root width; CH = canine height; M^1 L = length of the upper first molar; M^1 W = width of the upper first molar; M_1 L = length of the lower first molar; M_1W = width of the lower first molar; M = male; F = female. Measurements of the molar taken as defined in Gingerich et al. (1982). All measurements in millimeters (mm).

immediate vasculature) and the surface area of the neocortex were measured in Avizo 8.1. The neocortical surface was selected using the surface editor and was defined as the cerebral surface caudal to the circular fissure separating the olfactory bulbs from the cerebrum, dorsal to the position of the orbitotemporal canal, and rostral to the transverse sinus. Thus, the neocortical surface area did not include the dorsal surface area of the olfactory bulbs but did include that of the superior sagittal sinus. Following Long et al. (2015), neocortical ratio was calculated as the ratio of neocortical surface area to total endocast surface area.

3.7. Body mass predictions

In order to standardize how body mass was predicted and to compare the effects of using different equations on estimated EQs, body masses for these eight specimens were predicted using results from several published body mass prediction equations (SOM Table 2). In order to test the predictive accuracy of these equations, the PRESS statistic (predicted residual sum of squares; Allen, 1974; Smith, 2002), a leave-one-out cross-validation method, was calculated using the original reference samples of all equations (except the cranial length equation of Martin, 1990). To compensate for differing sample sizes, root mean squared prediction error (PRESS RMSE = $\sqrt{}$[PRESS/n]) was also calculated. Both PRESS and PRESS RMSE are reported in SOM Table 2.

3.7.1. Predictions based on dental measures All specimens preserve an upper first molar, so the length and width of the M^1 from each specimen (Table 3) were used to calculate occlusal area following Gingerich et al. (1982). When available, the length and width of M_1 were also measured (Table 3). If the specimen preserved both the right and left teeth, then the average area of both sides was used. Body masses for each specimen were predicted using results from all-primate-except-*Tarsius* (Gingerich et al., 1982) and strepsirrhine-only (Dagosto and Terranova, 1992) regressions of M^1 and M_1 occlusal areas to extant species mean body mass. As a small bias is introduced when data are back-transformed from logarithmic to arithmetic scales (Smith, 1993), quasi-maximum likelihood correction factors were applied to both sets of dental body mass prediction equations (Gingerich et al., 1982; Dagosto and Terranova, 1992).

3.7.2. Predictions based on cranial measures Body mass was predicted using both the vertical and horizontal phylogenetic Generalized Least Squares regression (vertical pGLS and horizontal pGLS) equations of Silcox et al. (2009a) for three specimens of *N. tenebrosus* (AMNH 127167, USNM V 23277, and USNM V 23278), two specimens of *S. gracilis* (USNM V 17994 and USNM V 21815), and one specimen of *A. parisiensis* (NHM M 1345). Vertical pGLS or horizontal pGLS use reference samples of cranial lengths of prosimian taxa that prefer vertical or horizontal postures, respectively, at rest (Silcox et al., 2009a). Body mass was also predicted for these specimens using the generalized primate cranial length regression from Martin (1990). Correction factors for bias introduced when de-transforming data were not available for these analyses. Measured cranial lengths are reported in Table 4. Further details on how cranial length was measured are reported in the SOM.

3.7.3. Predictions based on postcranial measures *Notharctus tenebrosus* has larger molars than those of *S. gracilis*, while sharing similar cranial length (Tables 3 and 4; Gazin, 1958), suggesting the possibility that these two species were similar in body mass but that *N. tenebrosus* had relatively larger molars than *S. gracilis*. To explore this possibility using a different proxy, body mass predictions were calculated from the articular surface area of the astragalar ectal facet taken on surface reconstructions based on high-resolution X-ray μCT scans, and compared to those from cranial and dental measures. For USNM V 17994, the ectal facet area of the associated astragalus was used to predict body mass using the all-euarchontan equation of Yapuncich et al. (2015). Additionally, species mean body mass predictions were calculated using mean values from unassociated astragali attributed to *N. tenebrosus* ($n = 7$), *S. gracilis* ($n = 3$), and *A. parisiensis* ($n = 7$). Astragalar specimens attributed to *N. tenebrosus* include AMNH 11474, AMNH 11478L and 11478R, AMNH 11483, AMNH 12570, AMNH 129382, AMNH 131761, and AMNH 131945. Astragalar specimens attributed to *S. gracilis* include AMNH 131763, AMNH 131774R, and USNM 17994. Astragalar specimens attributed to *A. parisiensis* specimens include ISE-M-ECA-1379, ISE-M-ECA-7377, ISE-M-ROS2-708, MaPhQ 1390, MaPhQ unnumbered, VI ESC 936, and VI ROS 106. Scanning parameters/modalities for these specimens may be found in Boyer and Seiffert (2013) and Boyer et al. (2015). Surface files are available on morphosource.org and can be found by copying and pasting the appropriate specimen number into the search field.

For all specimens in the sample, brain volumes, predicted body masses, and calculated EQ estimates were compared to previously published results as well as those for extant and other extinct primates. Data from previous studies are from Radinsky (1977), Gurche (1978, 1982), Jerison (1979), Gingerich and Martin (1981), and Martin (1990). Body mass and brain volume data for extant taxa are from Isler et al. (2008). Olfactory bulb volume data for extant taxa are from Stephan et al. (1970). Data for plesiadapiforms are from Silcox et al. (2009b, 2010), and Orliac et al. (2014). Data for *R. viejaensis* are from Kirk et al. (2014), and those for *M. erinaceus* are from Ramdarshan and Orliac (2015).

Table 4
Cranial lengths of specimens in the sample.

Specimen	Species	Maximum length	Inion-I^2 length	Inion-C length	Length without nuchal crest
AMNH 127167	*N. tenebrosus*	78.5	78.5	69.2	–
USNM V 23277	*N. tenebrosus*	74.7	–	74.7	–
USNM V 23278	*N. tenebrosus*	68.1	–	68.1	–
USNM V 17994	*S. gracilis*	69.5	–	69.5	–
USNM V 17996	*S. gracilis*	63.9	–	–	–
USNM V 21815	*S. gracilis*	73.3	71.5	67.6	–
UM 32773	*S. gracilis*	59.7	–	59.7	–
NHM M 1345	*A. parisiensis*	85.0	–	85.0	75.6

Inion-I^2 length describes the length from the most caudal point of the cranium (inion) to just caudal of the upper second incisor on the sagittal plane. Inion-C length describes the length from the inion to just caudal to the canine on the sagittal plane. For all specimens except AMNH 127167 and USNM V 21815, the maximum cranial length is equal to the Inion-C length. For AMNH 12767, maximum cranial length is equal to Inion-I^2 length. In USNM V 21815, maximum cranial length is equal to the distance from inion to the most rostral point on the premaxilla (prosthion). Because NHM M 1345 is the only specimen with a pronounced nuchal crest, cranial length was also measured without the length of the nuchal crest included in the sagittal plane for this specimen.

4. Results

4.1. Developmental stage of UM 32773

The eruption sequence of the right dentary of UM 32773 is compared to the mandibular eruption sequence of *S. sciureus* and *D. masillae* in Figure 3. Compared to *D. masillae*, the upper teeth of UM 32773 are similar in having an erupting canine, dP^3 and dP^4 with P^3 and P^4 forming, and a fully erupted M_1. There is evidence that UM 32773 was more mature, however, as the M^2 is still erupting and the M^3 is erupting without roots in *D. masillae*, while the M^2 is fully erupted and M^3 is erupting with roots in UM 32773. However, the $P\frac{2}{2}$ of *D. masillae* are fully erupted, while these teeth are beginning to erupt in UM 32773. These contrasting patterns suggest that premolar eruption sequences were different in *S. gracilis* and *D. masillae*. If the dental eruption sequences and growth trajectories of *S. gracilis* and *S. sciureus* are comparable, it suggests that the brain mass of UM 32773 was just over 98% of its adult brain mass, and that the body mass was approximately 63%–64% of its adult body mass. However, if *S. gracilis* had followed a more strepsirrhine-like growth trajectory, it is likely that the percentage of adult body mass achieved by UM 32773 at the time of death was higher. López Torres et al. (2015) found that strepsirrhine growth models predicted that *D. masillae* had reached 75.6%–78% of the adult body mass (compared to 60% using the *S. sciureus* model). Considering that the *D. masillae* specimen was apparently less mature than UM 32773, it is probable that this *S. gracilis* specimen had reached a higher percentage of body mass than *D. masillae*, so, following a strepsirrhine-like growth model, would have weighed more than 78% of the adult body mass.

4.2. Sex of the specimens

Upper canine measurements for all specimens which could be measured are recorded in Table 3. When compared to previously reported canine dimensions for *N. tenebrosus* (Alexander, 1994), the upper canine dimensions of USNM V 23277 and USNM V 23278 are small, falling outside the range of variation for males, suggesting that these individuals were females. Both specimens possess a low sagittal crest and rounded, non-triangular posterior edge of the coronal suture (SOM Fig. 1C, E), which have been suggested as cranial features of female *N. tenebrosus* (Alexander, 1994). In addition, while the zygomatic arch of USNM V 23277 is slightly crushed laterally, the face is narrower and the zygomatic is less flared than in the male AMNH 127167. Overall, the facial morphology of USNM V 23277 is more similar to that of the female AMNH 11466 (Gregory, 1920; Alexander, 1994).

Regarding the *S. gracilis* sample, canine dimorphism was not previously proposed to strongly distinguish males and females (Alexander, 1994). Cranial features of USNM V 21815 (assigned as female by Alexander, 1994) are more similar in appearance to those of USNM V 17996 than those of USNM V 17994 (SOM Fig. 1I, M). Specifically, the fact that temporal lines of USNM V 17996 do not meet until almost the lambdoidal suture would lead to a female diagnosis for that specimen according to Alexander (1994). The sex of UM 32773 (SOM Fig. 1O, P) could not be assessed because 1) the adult upper and lower canines were unerupted at the time of death (with juvenile canines not preserved), 2) the zygomatic arches are poorly preserved, 3) the temporal lines are ill-defined, and 4) the absence of a sagittal crest may be attributable to the individual's juvenility.

The following descriptions focus on aspects of the endocasts that appear derived or interesting from the perspective of morphological trends in primate brain evolution. In the SOM, we have provided a more comprehensive description, including information on many of the more general mammalian features of the endocasts of *N. tenebrosus* and *S. gracilis*.

4.3. Description of the virtual endocasts of N. tenebrosus

All three virtual endocasts of *N. tenebrosus* (Fig. 4) preserve some portion of the rostral-most part of the brain, the olfactory bulbs, followed by a circular fissure separating them from a cerebrum consisting of ill-defined frontal, temporal, and occipital lobes. None of the specimens has a cerebrum that overlaps the olfactory bulbs or cerebellum. The midbrain is not exposed at the juncture of the occipital lobe and the cerebellum in any of the *N. tenebrosus* endocasts, because it is covered by the transverse sinus and occipital lobe (Figs. 4 and 5B). AMNH 127167 (Figs. 4, 5, and 7, SOM Fig. 2) is the most complete of the *N. tenebrosus* endocasts, with only minor damage to the rostral-most part of the olfactory bulbs. USNM V 23277 is missing some of the rostral and ventral parts of the olfactory bulbs and has poor preservation of the ventral paleocortex (Figs. 4 and 7, SOM Fig. 3). USNM V 23278 has a better-preserved dorsal and ventral cerebral surface than that of USNM V 23277, but lacks portions of the cerebellum as well as rostral and ventral portions of the olfactory bulbs (Figs. 4 and 7, SOM Fig. 4).

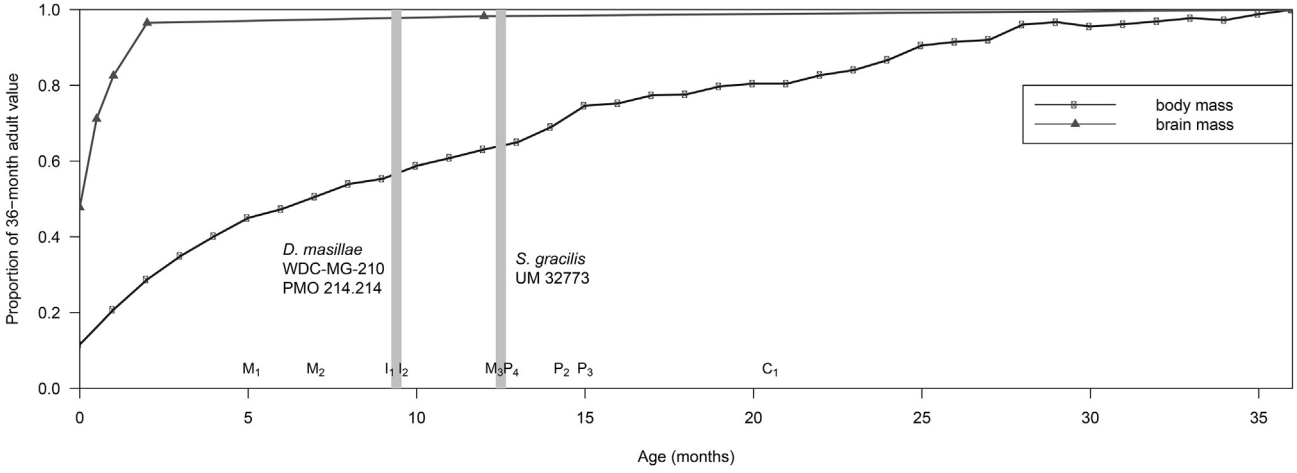

Figure 3. Hypothetical proportion of adult body mass and brain mass achieved by the juvenile *S. gracilis* specimen UM 32773 at death compared to growth in *Saimiri sciureus*. Dental eruption and body weight data from Long and Cooper (1968), brain weight data from Manocha (1979), and data for "Ida", the holotype specimen of *Darwinius masillae* (WDC-MG-210 and PMP 214.214) from Franzen et al. (2009).

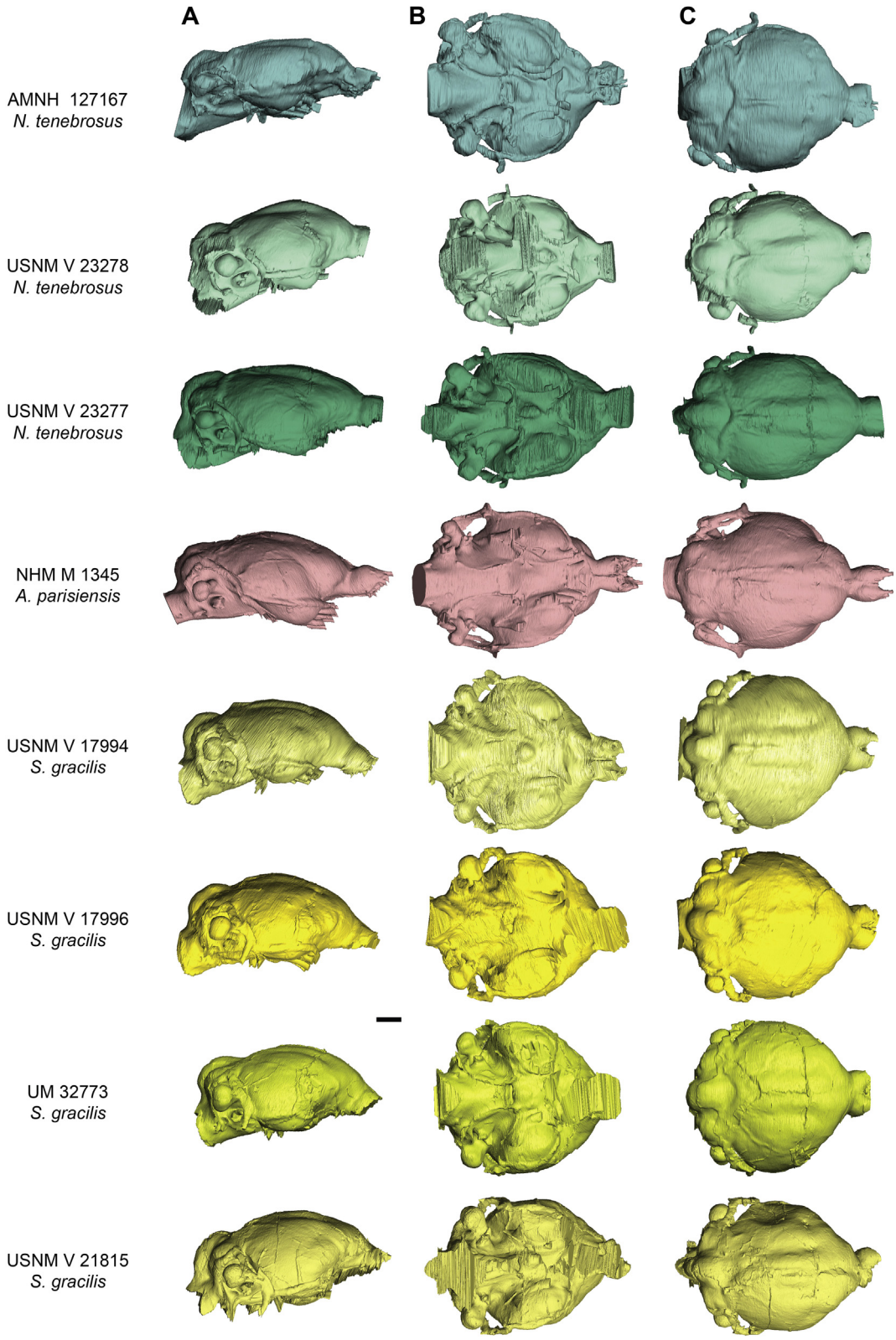

Figure 4. Endocasts in the sample in A) right lateral, B) ventral, and C) dorsal views. Scale bar = 5 mm.

The outlines of the three virtual endocasts of *N. tenebrosus* are variable due to differing proportions of the cerebrum. The greatest differences among the endocasts are in the ratio of maximum width to maximum length and the ratio of maximum height to maximum width (Fig. 6 and Table 5). The absolutely laterally broadest and dorsoventrally flattest endocast is AMNH 127167, which is reflected in its very high value for the ratio of width:length and its very low value for the ratio of height:width (Fig. 6). Overall, USNM V 23277 is

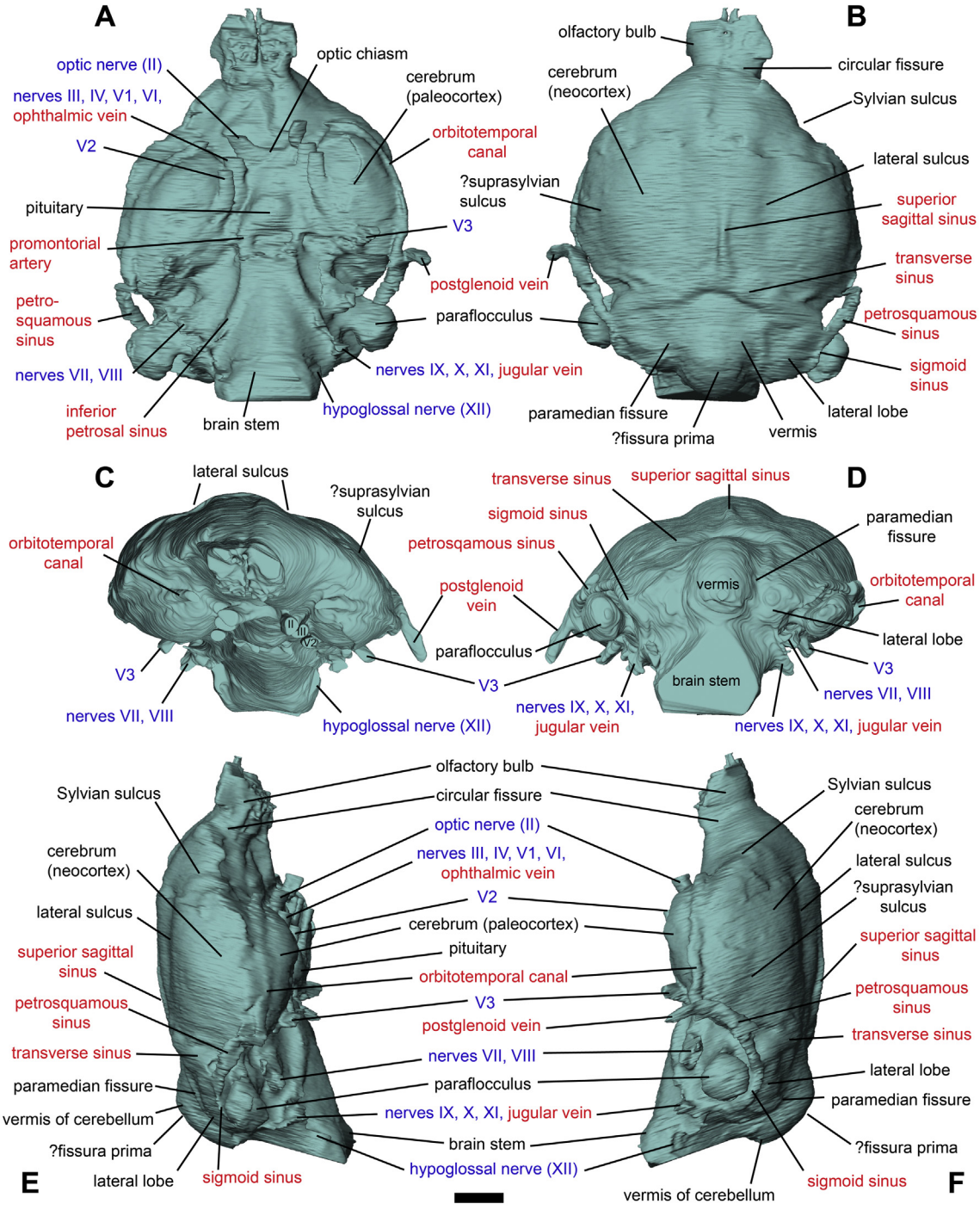

Figure 5. Virtual endocast of *Notharctus tenebrosus* (AMNH 127167) in A) ventral, B) dorsal, C) anterior, D) posterior, E) right lateral, and F) left lateral views. Scale = 5 mm. Features only tentatively identified are indicated with a question mark.

more rostro-caudally elongate than USNM V 23278 and AMNH 127167, reflected in its low value for the width:length ratio (Fig. 6). The maximum height:length ratio is less variable, although it is worth noting that the longest (USNM V 23277) and the shortest (USNM V 23278) endocasts actually have the same width (Table 5), reflecting the fact that there is notable variation in these relative proportions as well.

Due to poor preservation, it cannot be determined whether the olfactory bulbs of *N. tenebrosus* were "bilobed" or "bifurcated" (sensu Takai et al., 2003, p.140), although numerous casts of nerve roots leading through the cribriform plate of the ethmoid bone may be observed on the olfactory bulbs of AMNH 127167 (Fig. 5A, SOM Fig. 2) demonstrating good preservation of the ventral face of the bulbs in this specimen. The rostral-most portion of the olfactory bulbs in all the *N. tenebrosus* specimens in the sample terminate past the caudal edge of the postorbital bars (Fig. 7, SOM Figs. 2–4).

Elliot Smith (1902) defined the Sylvian sulcus as originating at the rostral end of the rhinal sulcus (presumably under the orbitotemporal canal in these endocasts) and continuing dorsally and caudally along the temporal lobe. On each endocast, shallow

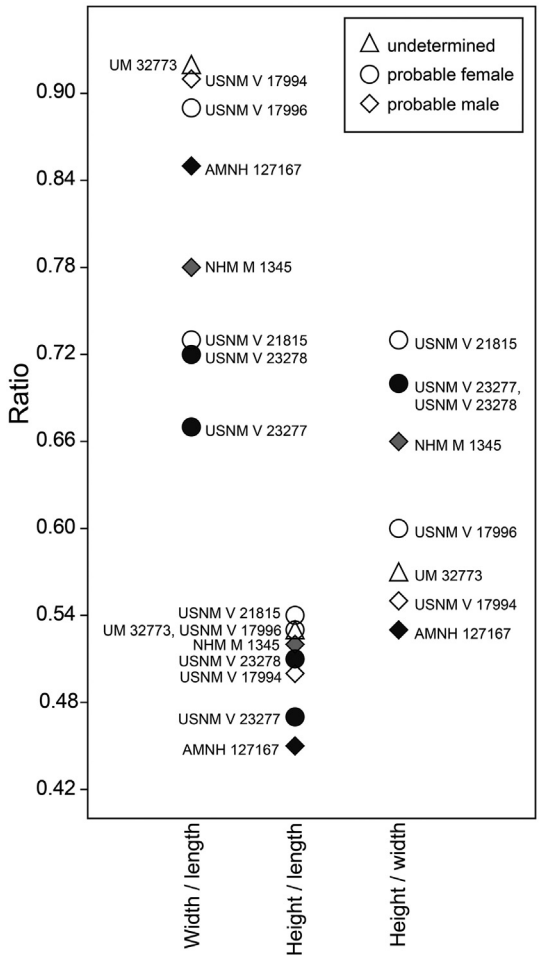

Figure 6. A plot comparing the maximum endocast ratios of the specimens in the sample. Black markers belong to specimens of *N. tenebrosus*, gray markers belong to specimens of *A. parisiensis*, and unfilled markers belong to specimens of *S. gracilis*. Ratios are reported in Table 5.

bilateral depressions on the dorsal outline of the anterior cerebrum are identifiable as Sylvian sulci (Figs. 4 and 5B, E, F). These sulci are better defined ventrally and intersect the rhinal fissure (overlain by the orbitotemporal canal). Dorsally, the Sylvian sulci manifest as shallow depressions in all three specimens (Fig. 4). Evidence for the suprasylvian sulcus is variable. It may be identified on AMNH 127167 (Fig. 5B) as a shallow sulcus on the dorsal surface of the cerebrum paralleling the lateral borders of the temporal lobes. This feature is better defined on the left side of AMNH 127167 than the right, and is absent in USNM V 23277 and USNM V 23278. While AMNH 127167 does not preserve casts of the meningeal vessels on the cerebrum, the other two *N. tenebrosus* specimens possess several casts of branching meningeal vessels that extend caudally on the temporal lobes.

The cerebrum can be divided into several parts. The frontal lobes may be approximated as the portion of the cerebrum rostral to the Sylvian sulcus. The temporal lobes are caudal to the Sylvian sulcus, and merge posteriorly into the occipital lobes. AMNH 127167 has rostro-caudally short frontal lobes and a laterally wide temporal lobe, while USNM V 23277 has rostro-caudally longer frontal lobes and a laterally narrower temporal pole (Fig. 4). This difference is evinced by maximum cerebral width to length ratios: AMNH 127167 has the shortest cerebrum relative to width at 1.28, while USNM V 23277 has the most elongate cerebrum at 0.95. At 1.05, USNM V 23278 is intermediate (Table 5).

4.4. *Descriptions of the virtual endocasts of* S. gracilis

The virtual endocasts of USNM V 17994 (Figs. 4, 7, and 8, SOM Fig. 5), USNM V 17996 (Figs. 4 and 7, SOM Fig. 6), USNM V 21815 (Figs. 4 and 7, SOM Fig. 7), and UM 32773 (Figs. 4 and 7, SOM Fig. 8) are similar in having heart-shaped cerebra with a tapering frontal region, an expanded temporal pole, and a rounded occipital region. However, the cerebrum of the endocast of USNM V 21815 has a concave depression on the left temporal lobe, corresponding to a depression on the external surface of the parietal bone (SOM Fig. 7G, H). None of the endocasts has a cerebrum that overlaps the cerebellum or olfactory bulbs (Fig. 4). None of the *S. gracilis* specimens exhibits midbrain exposure at the juncture of the occipital lobe and the cerebellum, due to overlap of the midbrain by the occipital lobe.

It could be argued that the relatively small endocast volume of USNM V 21815 is the result of damage to the specimen as the left cerebrum is dented and the right olfactory bulb is incomplete. To address this, we mirrored the undamaged right cerebrum and the more complete left olfactory bulb, and recalculated total endocranial volume. Indeed, the result (7.55 cm^3) is higher, but still volumetrically smaller than that of the other *S. gracilis* specimens in the sample (Table 5).

Relative proportions of USNM V 17994, USNM V 17996, and UM 32773 are fairly similar, particularly in width:length and height:width ratios (Table 5 and Fig. 6). While the height:length ratio of USNM V 21815 (0.54) is similar to that of the other *S. gracilis* endocasts, the maximum width:length ratio (0.73) and height:width ratio (0.73) indicate different proportions than other specimens in the sample. In those two latter ratios, USNM V 21815 is more similar to the ratios calculated for the two female *N. tenebrosus* specimens, USNM V 23277 and USNM V 23278.

The virtual endocasts of USNM V 17994, USNM V 17996, and UM 32773 preserve mostly complete olfactory bulbs (Fig. 4). USNM V 21815 is not well preserved on the rostral-most portion of the endocast with most of the right olfactory bulb missing (SOM Fig. 7). The olfactory bulbs of USNM V 17994 are complete: the bulbs are bifurcate, show many small casts of olfactory nerve foramina branching off into the cribriform plate (Fig. 8A), and are separated from the cerebrum by a shallow circular fissure that is better defined on the lateral aspects than in the dorsal or ventral aspect (Fig. 8). While casts of the olfactory bulbs of USNM V 17996 and UM 32773 are less well preserved ventrally and rostrally, they are bifurcate in dorsal view (SOM Figs. 6 and 8). The rostral-most aspect of the olfactory bulbs terminates caudal to the rostral edge of the postorbital bar in specimens that preserve the postorbital bar (USNM V 17994 and USNM V 21815; Fig. 7, SOM Figs. 5 and 7).

The Sylvian sulci are absent on UM 32773 and USNM V 17996 (Fig. 4, SOM Figs. 6 and 8). The other two *S. gracilis* specimens, USNM V 17994 (Fig. 8, SOM Fig. 5) and USNM V 21815 (SOM Fig. 7), preserve shallow indentations rostral and lateral to the lateral sulci that may be Sylvian sulci. These are somewhat better defined on USNM V 21815, which preserves this feature bilaterally. On USNM V 17994, a potential Sylvian sulcus is more apparent on the left side (Fig. 8E), and the right side has a cast of a possible vessel in the same region (Fig. 8F). Other casts of possible vessels are present on the right side of UM 32773 and the left side of USNM V 17996 where a Sylvian sulcus would be expected (SOM Figs. 6 and 8).

4.5. *Description of the virtual endocast of* A. parisiensis

The endocast of NHM M 1345 and morphology of the endocasts of *A. parisiensis* has been previously described (Neumayer, 1906; Gregory, 1920; Le Gros Clark, 1945; Radinsky, 1970; Gurche, 1978, 1982; Gingerich and Martin, 1981; Martin, 1990) and will not be

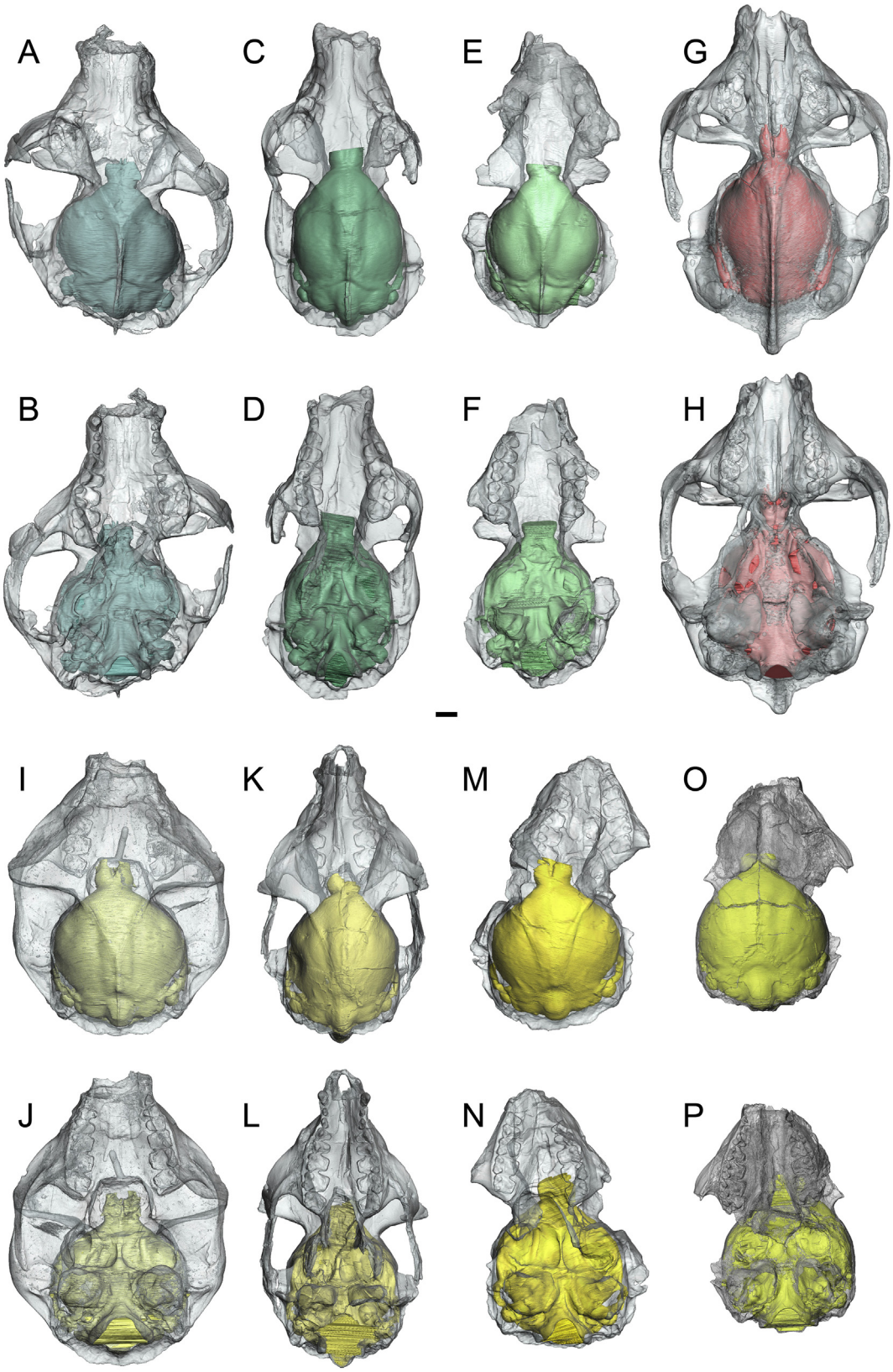

Figure 7. Dorsal and ventral views, respectively, of the virtual endocasts of A and B) *Notharctus tenebrosus* (AMNH 127167), C and D) *N. tenebrosus* (USNM V 23277), E and F) *N. tenebrosus* (USNM V 23278), G and H) *Adapis parisiensis* (NHM M 1345), I and J) *Smilodectes gracilis* (USNM V 17994), K and L) *S. gracilis* (USNM V 21815), M and N) *S. gracilis* (USNM V 17996), and O and P) *S. gracilis* (UM 32773) within transparent renderings of their crania.

Table 5
Measurements of the virtual endocasts in the sample.

	Notharctus tenebrosus			*Smilodectes gracilis*				*Adapis parisiensis*
	AMNH 127167	USNM V 23277	USNM V 23278	USNM V 17994	USNM V 17996	USNM V 21815	UM 32773	NHM M 1345
Total endocast length	40.9	42.7	38.1	40.2	40.7	40.0	36.8	45.7
Maximum endocast width	29.7	25.5	25.2	30.8	30.3	24.8	30.5	36.6
Maximum endocast height	15.7	17.7	17.7	16.9	18.2	18.2	17.4	19.0
Olfactory bulb length	6.17	4.82	3.29	6.32	6.69	4.31	3.80	9.09
Olfactory bulb width	8.97	8.17	8.28	9.11	9.07	7.94	9.19	7.54
Length of the endocast without olfactory bulbs	34.8	37.8	34.8	33.9	34.0	33.9	32.9	36.6
Olfactory bulb length/total endocast length	0.15	0.11	0.09	0.16	0.16	0.11	0.10	0.20
Endocast width/total endocast length	0.72	0.60	0.66	0.77	0.74	0.62	0.83	0.63
Endocast width/length of the endocast without OB	0.85	0.67	0.72	0.91	0.89	0.73	0.92	0.78
Endocast height/total endocast length	0.38	0.42	0.46	0.42	0.45	0.46	0.47	0.42
Endocast height/length of the endocast without OB	0.45	0.47	0.51	0.50	0.53	0.54	0.53	0.52
Endocast height/width ratio	0.53	0.70	0.70	0.55	0.60	0.73	0.57	0.66
Maximum length of cerebrum	23.1	25.9	24.6	24.5	24.3	24.7	24.0	27.0
Endocast width/cerebral length ratio	1.28	1.05	0.95	1.26	1.24	1.00	1.27	1.07
Total endocast volume	7380	8060	7430	8630	8990	7440	8420	8810
Volume of olfactory bulbs	155	180	112	178	150	92.2	130	212
% of endocast composed of olfactory bulbs	2.10	2.23	1.51	2.06	1.67	1.24	1.54	2.40
Maximum width of cerebellar portion	20.0	17.6	–	17.7	18.1	16.3	18.7	15.7
Maximum cerebellar width/maximum endocast width	0.68	0.69	–	0.58	0.60	0.66	0.61	0.55
Hypophysis length	3.17	4.22	4.46	4.00	4.51	4.65	3.48	5.90
Hypophysis width	4.73	2.49	2.91	3.75	3.68	3.55	3.44	4.80
Hypophysis depth	1.01	1.84	1.32	1.72	1.65	2.10	0.57	0.72
Hypophysis length/hypophysis width ratio	0.67	1.69	1.53	1.07	1.23	1.31	1.01	1.23
Distance of midpoint of hypophysis to anterior edge of optic chiasm	5.71	–	5.28	7.20	7.91	–	6.04	10.83
Total endocast surface area	2880	3090	2920	3500	3300	3100	2990	3170
Surface area of olfactory bulbs	165	177	136	213	256	157	183	195
Surface area of the neocortex	832	973	911	1070	1030	1010	1020	986
Neocortical ratio (without olfactory bulb surface area)	0.31	0.33	0.33	0.33	0.34	0.34	0.36	0.33

Lengths are in millimeters (mm), areas are in mm^2, and volumes are in mm^3. OB = olfactory bulbs. Length of cerebrum was measured in the dorsal view from the posterior edge of the transverse sinus where it intersects the superior sagittal sinus to the posterior edge of the circular fissure. Total endocast volume does not include the volume of the postglenoid vein. Maximum width of the cerebellar portion does not include the sigmoid sinus.

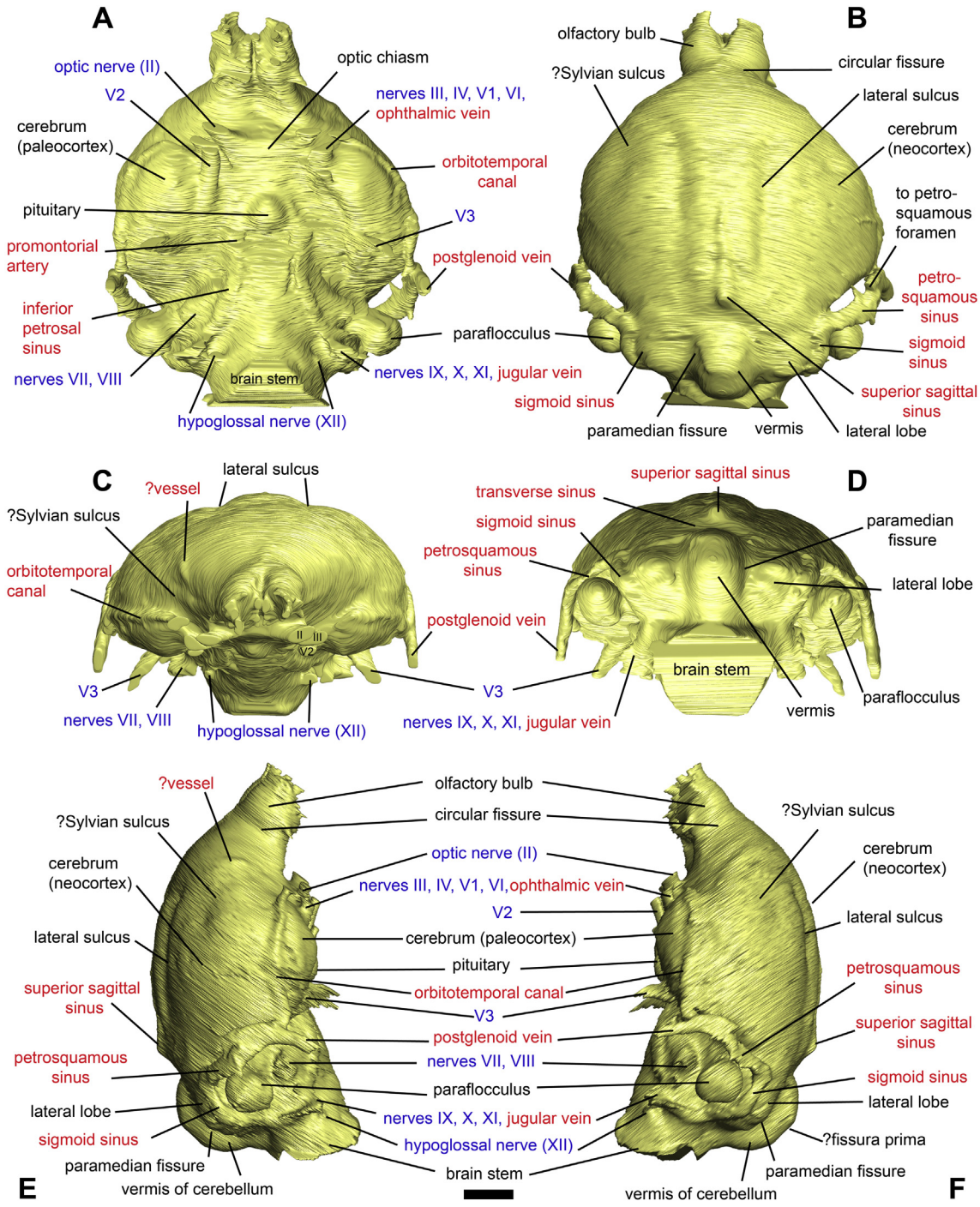

Figure 8. The virtual endocast of *Smilodectes gracilis* (USNM V 17994) in A) ventral, B) dorsal, C) anterior, D) posterior, E) right lateral, and F) left lateral views. Scale = 5 mm. Features only tentatively identified are indicated with a question mark.

re-described here in detail, as our findings are consistent with the previous descriptions. Overall, the virtual endocast of NHM M 1345 (Figs. 4, 7, and 9, SOM Fig. 9) is fairly complete, and reveals anatomy of the casts of the petrosquamous sinus and postglenoid foramen. The petrosquamous sinus was completely encased in two bony canals on the left side (Fig. 9A, B) and one on the right, and connects the contents of the postglenoid foramen with the contents of the canal to the foramen on the parieto-squamosal suture and the transverse and sigmoid sinus (Fig. 9E, F). The petrosquamous sinus is well-separated from the narrow occipital lobe of the cerebrum by thick bone (see Fig. 7 and SOM Fig. 9A). There are some faint casts of the meningeal vasculature preserved on the virtual endocast (Fig. 9).

The total volume of the virtual endocast is 8.81 cm^3 (Table 5), which is nearly identical to the volume previously reported for NHM M 1345 by infilling of the cranium with mustard seed (8.80 cm^3; Gingerich and Martin, 1981), and somewhat larger than the volume of 8.31 cm^3 reported by Gurche (1978, 1982) through water displacement of BM. M. 20192, an artificial endocast of NHM M 1345. Shrinkage during the casting of the latex endocast likely accounts for this small discrepancy in volume, as noted by Gingerich and Martin (1981). The olfactory bulbs are 0.212 cm^3, or

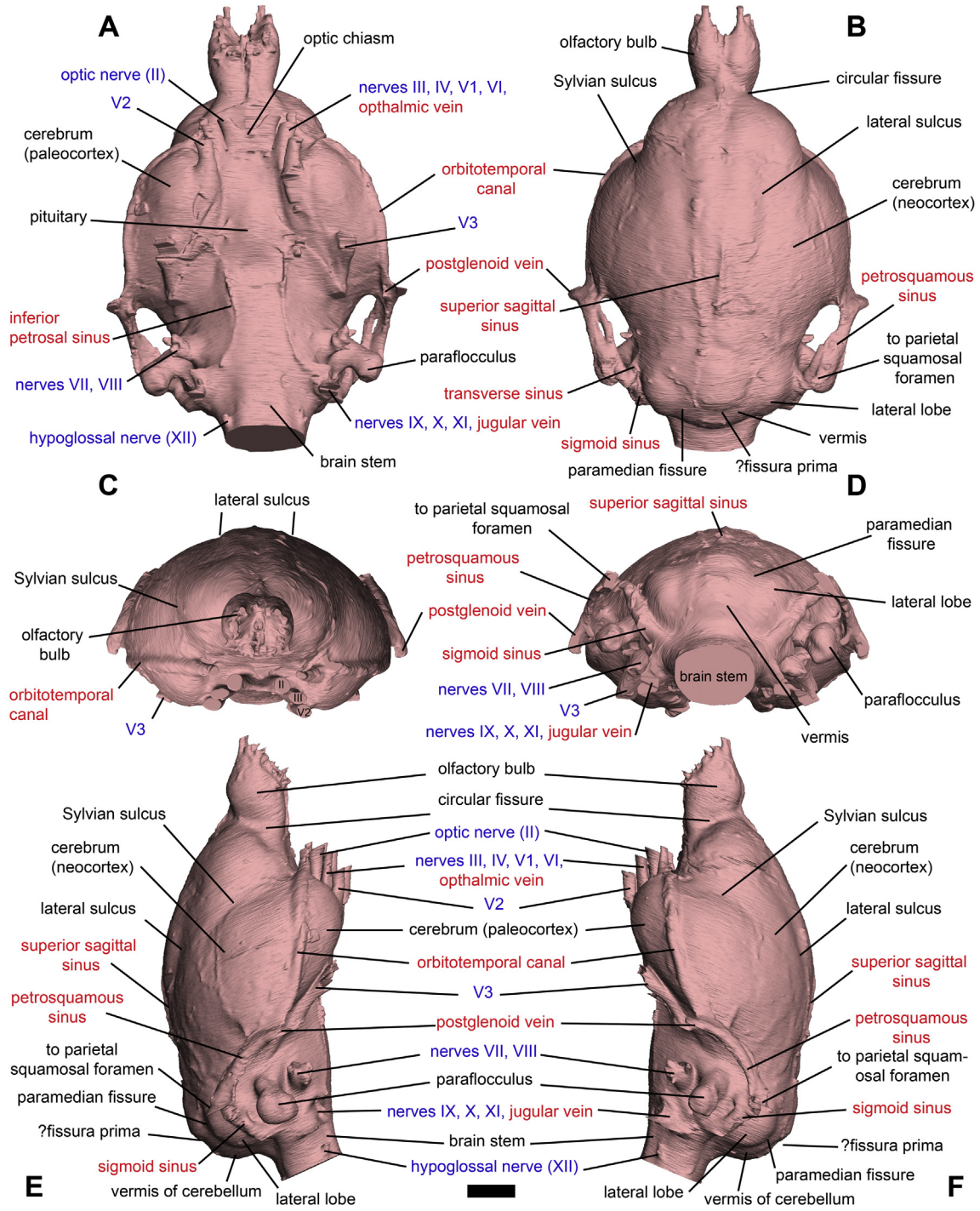

Figure 9. The virtual endocast of *Adapis parisiensis* (NHM M 1345) in A) ventral, B) dorsal, C) anterior, D) posterior, E) right lateral, and F) left lateral views. Scale = 5 mm. Features only tentatively identified are indicated with a question mark.

2.4% of the total volume, which is lower than the value estimated by Gurche (1982) for this specimen (0.267 cm^3, with a probable range from 0.265 cm^3 to 0.334 cm^3).

4.6. Predicted body masses

First upper molar (M^1) lengths and widths are reported in Table 3 and the resulting body mass predictions for each specimen are summarized in Table 6 and illustrated in Figure 10. Results using a regression of all-primate M^1 molar occlusal area on known body mass for a broad sample of extant primates (Gingerich et al., 1982) indicate higher body masses than one using only extant strepsirrhines (Dagosto and Terranova, 1992). For all specimens except USNM V 23278, Dagosto and Terranova's (1992) M^1 equation predicts a greater body mass than the M_1 equation. All dental body mass predictions for *N. tenebrosus* are consistently greater than those of *S. gracilis* (Fig. 10). Using the strepsirrhine-only M^1 equation of Dagosto and Terranova (1992), the body masses of the *N. tenebrosus* specimens in the sample range from 2244 g to 2923 g, while those of *S. gracilis* range from 1303 g to 1582 g.

Table 6
Body mass predictions and prediction intervals for specimens in the sample using different proxies.

Specimen	Species	G*M^1 (95% PI)	D&T M^1 (95% PI)	D&T M$_1$ (95% PI)	MSL	VPGLS (95% PI)	HPGLS (95% PI)	EFA (95% PI)
AMNH 127167	*N. tenebrosus*	5048 (1766, 14,428)	2641 (744, 9370)	2227 (867, 5720)	1910	1376 (526, 3602)	1795 (853, 3776)	–
AMNH 127167**					1171	979 (381, 2516)	1092 (523, 2281)	
USNM V 23277	*N. tenebrosus*	5576 (1951, 15,940)	2923 (820, 10,422)	2398 (931, 6172)	1577	1203 (463, 3125)	1476 (704, 3095)	–
USNM V 23278	*N. tenebrosus*	4302 (1505, 12,295)	2244 (637, 7903)	2604 (1009, 6722)	1099	937 (365, 2405)	1025 (491, 2140)	–
USNM V 17994	*S. gracilis*	2745 (959, 7856)	1420 (409, 4923)	–	1190	990 (385, 2547)	1111 (532, 2321)	2849 (1310, 6196)
USNM V 17996	*S. gracilis*	2525 (882, 7228)	1303 (377, 4510)	1185 (467, 3004)	–	–	–	–
USNM V 21815	*S. gracilis*	3053 (1067, 8730)	1582 (455, 5501)	1528 (600, 3891)	1460	1143 (442, 2961)	1370 (654, 2869)	–
USNM V 21815*					1324	1069 (414, 2759)	1242 (594, 2598)	
USNM V 21815**					1069	919 (359, 2356)	996 (477, 2078)	
UM 32773	*S. gracilis*	2998 (1045, 8546)	1547 (445, 5378)	1280 (504, 3249)	–	–	–	–
NHM M 1345	*A. parisiensis*	2088 (728, 5987)	1074 (311, 3703)	–	2602	1706 (641, 4536)	2456 (1160, 5200)	–
NHM M 1345***					1653	1243 (478, 3234)	1548 (738, 3247)	
Species sample mean	*N. tenebrosus* (M^1 n = 3; M$_1$ n = 3; "P–I" n = 3; EFA n = 7****)	4947 (1731, 14,140)	2587 (730, 9171)	2405 (934, 6191)	–	1158 (447, 3000)	1395 (666, 2923)	2902 (1342, 6347)
Species sample mean	*S. gracilis* (M^1 n = 4, M$_1$ n = 3, "P–I" n = 2; EFA n = 3****)	2820 (986, 8068)	1459 (420, 5062)	1323 (521, 3360)	–	1064 (375, 2474)	1234 (511, 2228)	2595 (1193, 5643)
Species sample mean	*A. parisiensis* (EFA n = 7****)	2088 (728, 5987)	1074 (311, 3703)	–	–	1706 (641, 4536)	2456 (1160, 5200)	1103 (507, 2397)

G*M^1 = all-primate upper first molar area equation from Gingerich et al. (1982); D&T M^1 = all-strepsirrhine upper first molar area equation from Dagosto and Terranova (1992); D&T M$_1$ = all-strepsirrhine lower first molar area equation from Dagosto and Terranova (1992); MSL = prosthion–inion ("P–I") primate cranial length equation from Martin (1990); VPGLS = vertical phylogenetic least squares regression calculated from cranial length of taxa preferring vertical resting postures from Silcox et al. (2009a); HPGLS = horizontal phylogenetic least squares regression calculated from cranial length of taxa preferring horizontal resting postures from Silcox et al. (2009a); EFA = euarchontan ectal facet area equation from Yapuncich et al. (2015). Equations using cranial length ("P–I") use maximum cranial length from prosthion to the alveolar rim just anterior to the third incisor; **, which uses cranial length from the prosthion to the maxillary/premaxillary suture just anterior to the canine; and *** which does not include the length of the nuchal crest projecting posterior to the occipital condyles. ****Includes ectal facet areas from specimens detailed in text. All masses are in grams (g). Equations are in SOM Table 2 and further explanations are in text.

Adapis parisiensis (NHM M 1345) has the lowest body mass when predicted from the same proxy and equation: 1074 g (Table 6).

Cranial length measurements are recorded in Table 4, and corresponding body mass predictions are given in Table 6. The generalized primate skull length equation from Martin (1990) yields higher body mass predictions than either the horizontal or vertical pGLS analyses of Silcox et al. (2009a,b). In contrast to results from the dentally-derived predictions, results from cranial data show *A. parisiensis* as having body mass higher than those of the notharctines. For example, using the Martin (1990) skull length equation, *A. parisiensis* yields a body mass prediction of 2602 g, but those of *N. tenebrosus* range from 1099 g to 1910 g and those of *S. gracilis* range from 1190 g to 1460 g. However, when the nuchal crest is not included in the cranial length, the predicted body mass of *A. parisiensis* drops to 1653 g, and overlaps the range of *N. tenebrosus*. Overlap between *A. parisiensis* and *N. tenebrosus* is also recovered using the horizontal and vertical pGLS analyses. In general, the horizontal pGLS analysis results in greater body mass prediction than those from the vertical pGLS analysis. All three cranial length predictions reveal an overlap in the range of predicted body mass for *N. tenebrosus* and *S. gracilis*. This remains true when shorter cranial lengths (which do not include the length of the premaxilla) are used for USNM V 21815 and AMNH 127167.

Of the specimens in the sample, the all-Euarchonta astragalar ectal facet area equation (Yapuncich et al., 2015) could be used to predict body mass for only one individual, USNM V 17994 (a male *S. gracilis*). For this specimen, the predicted body mass (2849 g; 95% PI: 1310–6196 g) was similar to that generated by the Gingerich et al. (1982) M^1 equation (2811 g; 95% PI 959–7856 g). While associated astragali were not recovered for specimens that yielded endocasts of *N. tenebrosus*, unassociated astragali of seven different individuals were measured and yielded a similar mean body mass estimate of 2902 g (95% PI: 1342–6347 g), within the range estimated for the *S. gracilis* specimen (USNM V 17994). Likewise, three additional astragali identified as those of *S. gracilis* but not associated with endocasts, were measured and yielded a mean body mass prediction of 2595 g (95% PI 1193–5643 g), slightly lower than the individual prediction for the *S. gracilis* specimen (USNM V 17994) but well within the 95% prediction interval.

4.7. Encephalization quotients (EQs)

Estimated Eisenberg EQs for specimens in this study are reported in Table 7 and plotted in Figure 10. Values were also calculated using the Jerison (1973) EQ equation, and are reported in Table 7 for comparability with other studies, but the following discussion focuses on the values calculated using the Eisenberg (1981) equation. When dental proxies are used, individuals of *S. gracilis* have consistently higher EQs than individuals of *N. tenebrosus*. The lowest EQs for *N. tenebrosus* specimens were calculated based on body masses predicted from the Gingerich et al. (1982) M^1 equation (0.24–0.28). Eisenberg's EQs calculated for *N. tenebrosus* using body masses predicted from the Dagosto and Terranova (1992) M^1 equation (0.40–0.45) were similar to those calculated using body masses predicted from the M$_1$ (0.40–0.46) equations. Based on body masses calculated from dental proxies, for *S. gracilis*, EQs range from 0.36–0.50 (Gingerich et al., 1982 M^1) to 0.58–0.81 (Dagosto and Terranova, 1992 M^1) and 0.60–0.87 (Dagosto and Terranova, 1992 M$_1$). *Adapis parisiensis* (NHM M 1345) has the highest EQs calculated for specimens in this sample using both of the M^1 body mass prediction equations (0.56, Gingerich et al., 1982 M^1; 0.92, Dagosto and Terranova, 1992 M^1).

Encephalization quotients calculated for *N. tenebrosus* and *S. gracilis* overlap when body mass is predicted from cranial length, although the range is shifted upwards for *S. gracilis* (Table 7 and

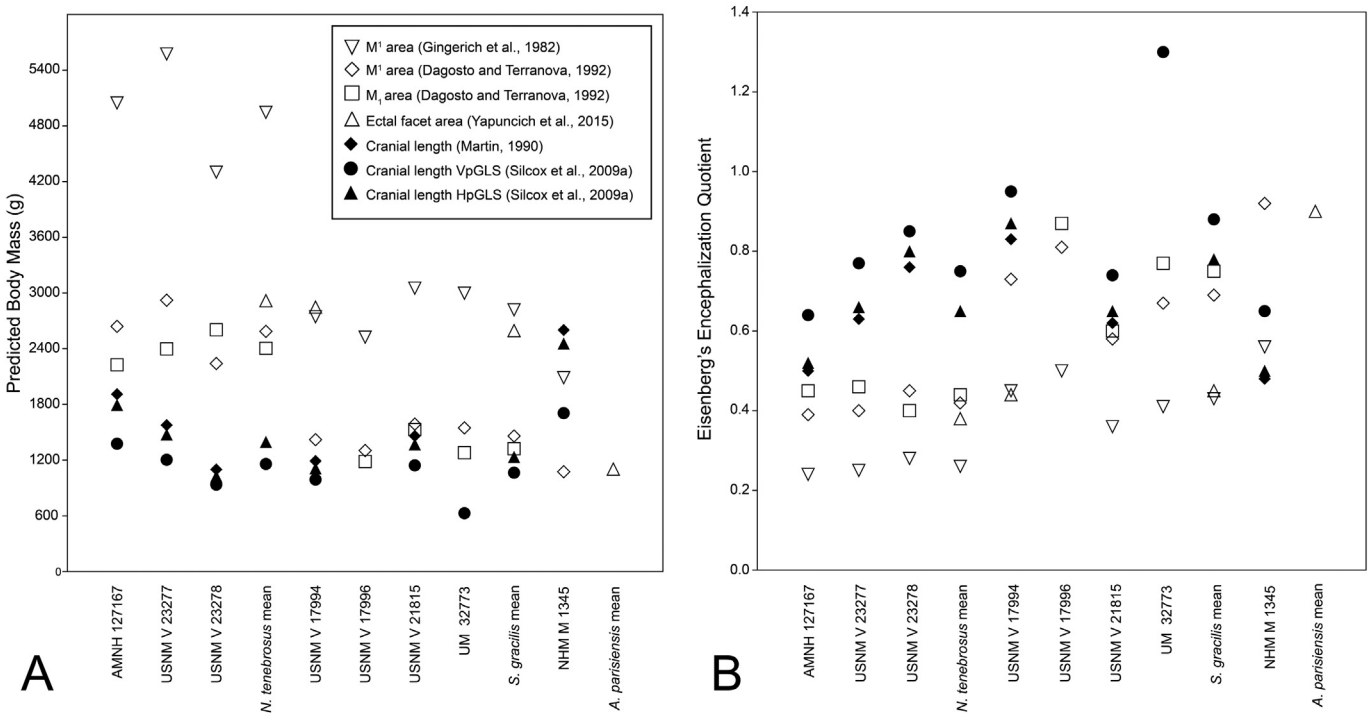

Figure 10. A) Comparison of body mass predictions calculated using different methods and B) comparison of Eisenberg's encephalization quotients (EQs) calculated using those body mass predictions. Equations used are from Table 2, body mass predictions are reported in Table 6, and Eisenberg's EQs are reported in Table 7. Cranial length VpGLS body mass prediction for UM 32773 was taken from Silcox et al. (2009a). For A, species means were calculated from the sample mean except when using ectal facet area (see Table 5) and for B, species mean EQs were calculated using the mean brain volumes of specimens in the sample.

Fig. 10B). Generally, the horizontal pGLS body mass predictions yield lower EQs than the vertical pGLS, while using Martin's (1990) analysis of cranial length yields the lowest EQs. None of the EQs calculated using body masses predicted from dental data for *N. tenebrosus* overlaps the EQs calculated from cranial length data for the same species. Estimates of EQ based on the various cranial length equations for *N. tenebrosus* range from 0.50 to 0.85, while EQ estimates for *S. gracilis* based on cranial length range from 0.62 to 0.95. When cranial lengths of AMNH 127167 (*N. tenebrosus*) and USNM V 21815 (*S. gracilis*) are reduced to exclude the premaxilla, the range becomes 0.63–0.85 for *N. tenebrosus* and 0.66–0.95 for *S. gracilis*. In contrast to the EQs calculated with body masses based on dental proxies, *A. parisiensis* generally has the lowest EQ when maximum cranial length is used to calculate body mass (Table 7). However, when the length of the nuchal crest is subtracted from the cranial length for *A. parisiensis*, the EQ falls within the range calculated for the *N. tenebrosus* and *S. gracilis* specimens in the sample. For example, using the Martin (1990) body mass prediction equation yields an EQ of 0.65 or 0.82 for NHM M 1345 when the nuchal crest length is included or excluded, respectively.

The EQ calculated for *N. tenebrosus* using the mean endocranial volume for this sample, and the mean body mass prediction for the sample of unassociated astragali based on astragalar ectal facet area (Yapuncich et al., 2015), is 0.38. This is most similar to the range of individual estimates derived from EQs calculated using the strepsirrhine-only analysis of Dagosto and Terranova (1992; M^1: 0.39–0.45; M_1: 0.40–0.46), well above the range calculated using the Gingerich et al. (1982) M^1 equation (0.24–0.28), and well below the range calculated based on cranial lengths (Table 8; 0.50–0.85). In contrast, the mean of EQ estimates using the unassociated

Table 7
Encephalization quotients of specimens in the sample.

Specimen	Species	G*M¹	D&T M¹	D&T M_1	MSL	VPGLS	HPGLS	EFA
AMNH 127167	*N. tenebrosus*	**0.24**/0.20	**0.39**/0.31	**0.45**/0.35	**0.50**/0.39	**0.64**/0.49	**0.52**/0.41	–
AMNH 127167**					**0.72**/0.54	**0.82**/0.61	**0.76**/0.57	
USNM V 23277	*N. tenebrosus*	**0.25**/0.21	**0.40**/0.32	**0.46**/0.37	**0.63**/0.48	**0.77**/0.58	**0.66**/0.51	–
USNM V 23278	*N. tenebrosus*	**0.28**/0.23	**0.45**/0.35	**0.40**/0.32	**0.76**/0.57	**0.85**/0.63	**0.80**/0.60	–
USNM V 17994	*S. gracilis*	**0.45**/0.36	**0.73**/0.56	–	**0.83**/0.63	**0.95**/0.71	**0.87**/0.65	**0.44**/0.35
USNM V 17996	*S. gracilis*	**0.50**/0.40	**0.81**/0.61	**0.87**/0.65	–	–	–	–
USNM V 21815	*S. gracilis*	**0.36**/0.29	**0.58**/0.44	**0.60**/0.46	**0.62**/0.47	**0.74**/0.55	**0.65**/0.49	–
USNM V 21815*					**0.66**/0.50	**0.78**/0.58	**0.69**/0.52	
USNM V 21815**					**0.78**/0.58	**0.87**/0.64	**0.87**/0.61	
UM 32773	*S. gracilis*	**0.41**/0.33	**0.67**/0.51	**0.77**/0.58	–	–	–	–
NHM M 1345	*A. parisiensis*	**0.56**/0.44	**0.92**/0.68	–	**0.48**/0.38	**0.65**/0.50	**0.50**/0.39	–
NHM M 1345***					**0.67**/0.51	**0.82**/0.62	**0.70**/0.54	
Species sample mean	*N. tenebrosus*	**0.26**/0.21	**0.41**/0.33	**0.44**/0.34	–	**0.75**/0.56	**0.65**/0.50	**0.38**/0.30
Species sample mean	*S. gracilis*	**0.43**/0.34	**0.69**/0.53	**0.75**/0.56	–	**0.88**/0.65	**0.78**/0.60	**0.45**/0.36
Species sample mean	*A. parisiensis*	–	–	–	–	–	–	**0.90**/0.67

First encephalization quotient (EQ) in bold is calculated using the equation of Eisenberg (1981) and the second EQ is calculated using the equation of Jerison (1973). Endocranial volumes and body masses used to calculate EQs are in Tables 5 and 6, respectively. Legend is the same as Table 6.

Table 8
Previous body mass predictions, endocranial volume, encephalization quotient, and calculation method for fossil primates.

Taxon	Specimen	BM (g)	BMPE	ECV	ECV method	EEQ	OBV	Source
N. tenebrosus	"Endocast A"	2500	CS	10.43	WD	0.58	236.60	3
	–	1990	CPM	10.40	F3	0.68	–	4
Smilodectes	–	2540	CSN	9.50	DGI	0.52	–	1
	–	1700	CSN	9.60	DGI	0.67	–	2
S. gracilis	YPM 12152	2500	CSN	9.95	WD	0.55	–	3
	USNM 23276	2400	CSN	9.12	WD	0.52	–	3
	–	1960	CPM	9.50	F3	0.63	–	4
Adapis	–	2540	CSN	9.00	DGI	0.49	–	1
	–	1700	CSN	9.00	DGI	0.67	–	2
A. parisiensis	BM M 20192	2500	CSN	8.31	WD	0.46	266.60	3
	–	2350	CPM	8.80	F5	0.51	–	4
	BMNH M 1345	2450	CPM2	8.80	MSV	0.50	–	5
	M 538	2350	CPM2	8.80	MSV	0.51	–	5
Rooneyia viejaensis	TMM 40688-7	373	MSL	7.23	DV	1.64	68.00	C
	TMM 40688-7	419	VPGLS	7.23	DV	1.51	68.00	6,10
	TMM 40688-7	332	HPGLS	7.23	DV	1.79	68.00	6,10
	TMM 40688-7	381	CPGLS	7.23	DV	1.62	68.00	6,10
	TMM 40688-7	1014	GM^1	7.23	DV	0.78	68.00	11
Microchoerus erinaceus	UM-PRR1771	241	MSL	4.26	DV	1.34	41.00	11
	UM-PRR1771	1150	GM^1	4.26	DV	0.42	41.00	11
Ignacius graybullianus	USNM 421608	286	MSL	2.41	DV	0.59	181.33	7
	USNM 421608		VPGLS	2.41	DV		181.33	C
	USNM 421608	253	HPGLS	2.41	DV	0.65	181.33	7
	USNM 421608	375	GM^1	2.41	DV	0.48	181.33	7
Microsyops annectens	UW 12362	1863	MSL	5.90	DV	0.41	300.55	8
	UW 12362		VPGLS	5.90	DV		300.55	C
	UW 12362	1710	HPGLS	5.90	DV	0.43	300.55	8
	UW 12362	2568	GM^1	5.90	DV	0.32	300.55	8
Plesiadapis tricuspidens	MNHM CR 125	6372	MSL	5.21	DV	0.12	136.00	9
	MNHM CR 125	2992	VPGLS	5.21	DV	0.25	136.00	C
	MNHM CR 125	5854	HPGLS	5.21	DV	0.15	136.00	C
	MNHM CR 125	2953	GM^1	5.21	DV	0.26	136.00	9

1 = Radinsky, 1977; 2 = Jerison, 1979; 3 = Gurche, 1982; 4 = Martin, 1990; 5 = Gingerich and Martin, 1981; 6 = Silcox et al., 2009a; 7 = Silcox et al., 2009b; 8 = Silcox et al., 2010; 9 = Orliac et al., 2013; 10 = Kirk et al., 2014; 11 = Ramdarshan and Orliac, 2015, C = calculated for current study; BM = body mass estimate in grams (g); BMPE = body mass prediction equation; CPGLS = estimated from cranial length using a "combined" phylogenetic least squares regression (combining taxa preferring vertical and horizontal resting postures) from Silcox et al. (2009a); CPM = took the mean of body masses estimated from cranial proxies of body mass from Martin (1990); CPM 2 = took the mean of body masses estimated from cranial proxies of body mass from Gingerich and Martin (1981); CS = compared to body mass of a similar sized modern primate analog using size of reconstructed skeleton; CSN = compared the reconstructed skeleton of *Notharctus* to a similar sized modern primate analog and assumed that the modern primate, *Notharctus*, and the specimen in question were approximately of the same body mass; DGI = double graphic integration; DV = volume extracted from a digital endocast; ECV = endocranial (endocast) volume in cubic centimeters (cm^3); EEQ = Eisenberg's encephalization quotient; GM^1 = estimated using body mass equation using M^1 area from Gingerich et al. (1982); F3 = from source 3 (Gurche, 1982); F5 = from source 5 (Gingerich and Martin, 1981); HPGLS = estimated from cranial length using a horizontal phylogenetic least squares regression calculated from taxa preferring horizontal resting postures from Silcox et al. (2009a); MSV = volume estimated from filling the cranial cavity with mustard seeds; MSL = generic primate cranial length body mass calculation equation from Martin (1990); OBV = olfactory bulb volume in cubic millimeters (mm^3); SS = judged to be slightly smaller in body mass than YPM 12152; VPGLS = estimated from cranial length using a vertical phylogenetic least squares regression calculated from taxa preferring vertical resting postures from Silcox et al. (2009a); WD = water displacement of reconstructed endocast.

sample of *S. gracilis* astragali (0.45) and the EQ of *S. gracilis* specimen USNM V 17994 calculated based on predicting body mass using the astragalus (0.44) are notably lower than those from other proxies (minimum value 0.58; Table 6), except for the M^1 equation of Gingerich et al. (1982; range of estimates 0.41–0.50). The EQ estimated from unassociated astragali of *A. parisiensis* (0.90) is higher than that of all individual associated estimates for NMH M 1345 except when body mass was predicted using the value calculated from the Dagosto and Terranova (1992) M^1 analysis (0.92).

4.8. Comparisons to EQs of other fossil primates

Body masses and EQs of plesiadapiforms, *R. viejaensis*, and adapiforms from previous studies are summarized in Table 8. Figure 11 illustrates a comparative plot of EQs for these taxa. Plesiadapiform EQs calculated with body mass predicted by the Gingerich et al. (1982) M^1 equation overlap with EQ values for *N. tenebrosus* and *S. gracilis* calculated here using the same body mass proxies (Table 7). Using predictions from the Martin (1990) cranial length data, plesiadapiform EQs also overlap with the EQ estimates calculated for *N. tenebrosus*. Plesiadapiform and *N. tenebrosus* EQs also overlap when body mass is predicted using the horizontal pGLS equation (Tables 7 and 8).

While results from calculating Eisenberg's EQ show no overlap between plesiadapiforms and extant strepsirrhines (0.86–2.46), the range of values of *S. gracilis* and *A. parisiensis* do overlap with that of extant strepsirrhines, depending on the body mass prediction equation used. Dental predictions for body mass produce EQs for *N. tenebrosus* that are lower than those for any extant primate, while predictions using cranial length yield EQs for *N. tenebrosus* that almost overlap with the lowest point plotted for extant strepsirrhines (maximum value 0.85 for USNM V 23278 using the vertical pGLS equation). None of Eisenberg's EQs for adapiforms included in this study, however, overlaps with the range known for extant haplorhines EQs (1.11–3.84). When mean body mass for the sample of unassociated astragali is predicted using astragalar ectal facet area, *A. parisiensis* is the only adapiform with a level of encephalization comparable to that of extant primates.

When the EQ of *R. viejaensis* is calculated using the volume estimate from Kirk et al. (2014) and the body mass predictions from the Gingerich et al. (1982) M^1 analysis, it falls within the range of EQs calculated for adapiforms in this study, but does not overlap with those of extant strepsirrhines. However, when EQ is calculated with body mass predicted from cranial length vertical pGLS, horizontal pGLS, and combined pGLS equations (Silcox et al., 2009a), the EQ of *R. viejaensis* (1.51–1.79) is above the range of adapiforms

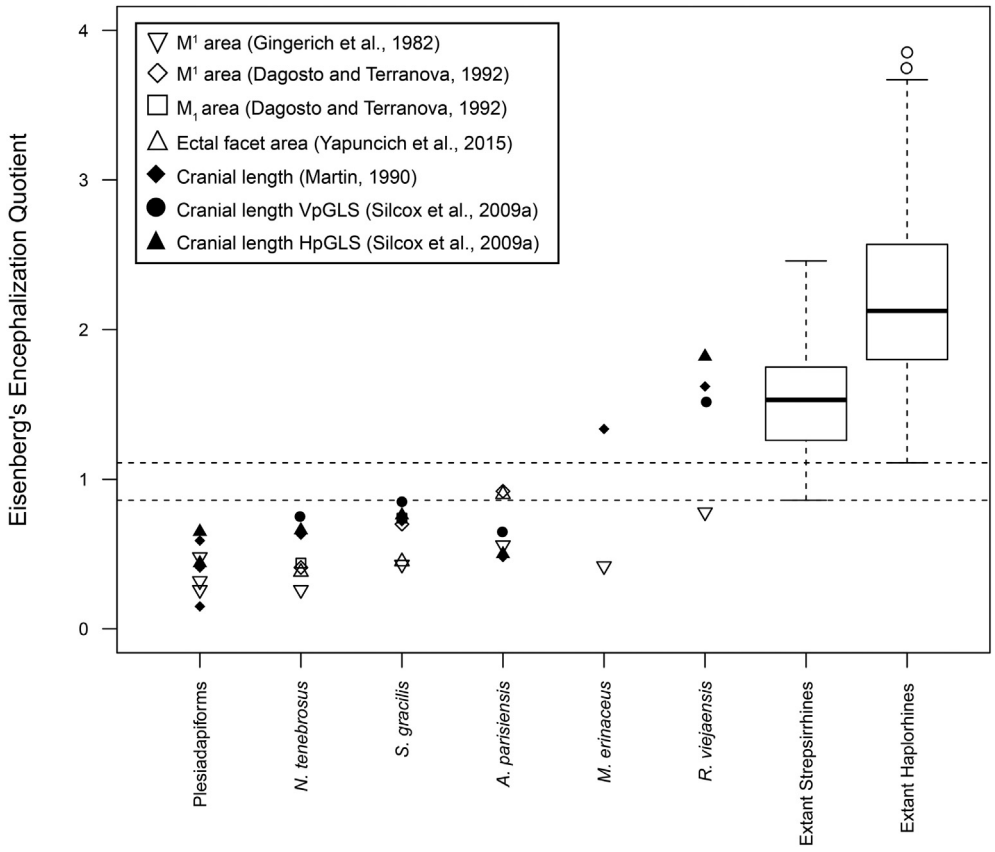

Figure 11. Comparison of Eisenberg's EQs of plesiadapiforms, early fossil euprimates, and extant strepsirrhines and haplorhines. EQs of plesiadapiforms taken from Silcox et al. (2009b, 2010), and Orliac et al. (2014), EQs of *Microchoerus erinaceus* taken from Ramdarshan and Orliac (2015), and EQs of *Rooneyia viejaensis* taken from Kirk et al. (2014) and calculated from body mass estimates from Silcox et al. (2009a). Data for extant taxa are from Isler et al. (2008). Data for adapiforms are from the current study (Table 7) and other species values are tabulated in Table 8.

in this study (regardless of which method for body mass prediction was used) and falls within the range of extant strepsirrhines and haplorhines.

The EQ of *M. erinaceus* is vastly different depending on the body mass proxy. When using the Gingerich et al. (1982) M^1 equation, its EQ falls below the range of extant strepsirrhines and falls within the range of dental EQs for the adapiforms in this sample. However, when cranial length is used, the EQ of *M. erinaceus* is within the range of extant haplorhines.

Generally, previously published EQs (Table 8) calculated for the adapiforms in this study are within the range of EQs calculated using all body mass prediction methods. Previously published EQs calculated for *N. tenebrosus* are most consistent with EQs calculated using cranially derived body masses, while past EQs for *S. gracilis* are somewhat more consistent with those calculated by dentally-derived body masses. Past EQs for *A. parisiensis* are similar to those calculated using body masses from the Gingerich et al. (1982) M^1, Martin (1990) cranial length, and Silcox et al. (2009a) horizontal pGLS equations.

4.9. Relative sizes of the olfactory bulbs

Volumes of the olfactory bulbs for *N. tenebrosus*, *S. gracilis*, and *A. parisiensis* are figured in a comparative context in Figure 12. Olfactory bulb volumes, brain volumes, and body masses plotted for extant taxa are for individuals unless otherwise noted in Stephan et al. (1970). Relative to total endocranial volume, the olfactory bulbs of both *N. tenebrosus* (AMNH 127167) and *S. gracilis* (USNM V 17996) fall within the minimum convex polygon characterizing extant strepsirrhines. Unlike the results of Kirk et al. (2014) and Ramdarshan and Orliac (2015), who found *Adapis* to plot outside of the minimum convex polygon of living strepsirrhines, the new virtual endocast of *A. parisiensis* (NHM M 1345) also plots within extant strepsirrhines. Figure 12 suggests that compared to plesiadapiforms, adapiforms in this sample have smaller olfactory bulb volume relative to total endocranial volume. However, the adapiforms have larger olfactory bulb volume relative to endocranial volume when compared to *R. viejaensis* and *M. erinaceus*.

When olfactory bulb volume is compared to body mass, a similar pattern emerges: *N. tenebrosus*, *S. gracilis*, and *A. parisiensis* fall within the minimum convex polygon characterizing extant strepsirrhines when body masses predicted from the Gingerich et al. (1982) M^1 equation are used. *Adapis parisiensis* has relatively larger olfactory bulbs than the notharctine adapiforms in the sample (Fig. 12). Plesiadapiforms have similarly-sized or larger olfactory bulbs relative to body mass compared to the adapiforms in the sample. *R. viejaensis* and *M. erinaceus* have smaller olfactory bulbs relative to body mass than either adapiforms or plesiadapiforms.

5. Discussion

5.1. Morphological comparisons

As might be expected for two closely related Eocene primates, the endocasts of *N. tenebrosus* and *S. gracilis* are generally similar to one another. Their small frontal lobes and lack of cerebral overlap onto either the olfactory bulbs or cerebellum are presumably

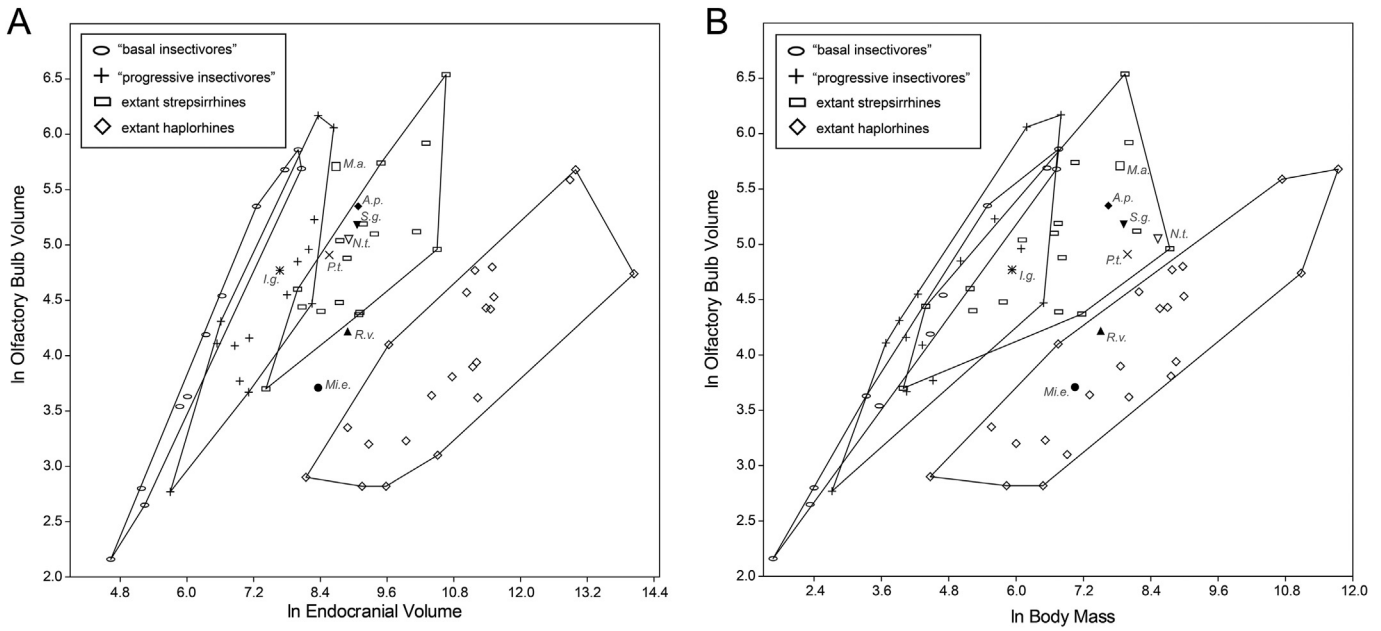

Figure 12. Natural log of olfactory bulb volume vs. natural log of A) total endocranial volume and B) body mass. Body masses of fossil taxa are those calculated using the Gingerich et al. (1982) upper M^1 equation. Abbreviations: *A.p.* = *Adapis parisiensis*; *I.g.* = *Ignacius graybullianus*; *M.a.* = *Microsyops annectens*; *Mi.e.* = *Microchoerus erinacius*; *N.t.* = *Notharctus tenebrosus*; *P.t.* = *Plesiadapis tricuspidens*; *R.v.* = *Rooneyia viejaensis*; *S.g.* = *Smilodectes gracilis*.

ancestral traits (Silcox et al., 2009b, 2010; Orliac et al., 2014) that both notharctine species share with the adapine *A. parisiensis* and with plesiadapiforms. In contrast, extant primates and *R. viejaensis* have cerebra that overlap both the olfactory bulb and cerebellum (Martin, 1990; Kirk et al., 2014). Fossil omomyiforms *Necrolemur antiquus*, *Tetonius homunculus*, and *M. erinaceus* have cerebra that overlap the cerebellum but not the olfactory bulbs (Radinsky, 1974; Gurche, 1982; Ramdarshan and Orliac, 2015). Cerebral overlap of the olfactory bulb is thought to signify frontal lobe expansion, though it is conceivably interpreted as simply a consequence of difference in head shape or the relationship between the splanchnocranium and neurocranium. Thus, while this assessment is qualitative and different possible explanations of cerebral overlap should be assessed more rigorously, plesiadapiform-like lack of cerebral overlap on the olfactory bulbs observed in the endocasts of adapiforms suggests that this group had frontal lobes that were less developed than in extant primates or omomyiforms. The significance of cerebral-cerebellar overlap is even less clear, as it may be related to basicranial flexion, brain expansion, or both (Silcox et al., 2010). In particular, the less flexed basicrania of adapiforms relative to *R. viejaensis* may partly explain the greater degree of cerebral overlap onto the cerebellum in the latter.

Notharctine endocasts differ from those of plesiadapiforms in having relatively wider, more globular temporal lobes and smaller olfactory bulbs relative to endocranial volume. Notharctines are similar to other euprimates in having no midbrain exposure at the juncture of the occipital lobe of the cerebrum and the cerebellum. It is uncertain if midbrain exposure, observed on several plesiadapiform endocasts, is primitive or secondarily derived (Edinger, 1964; Silcox et al., 2010), although the presence of exposure on some primitive euarchontoglirans (Silcox et al., 2011; Bertrand and Silcox, 2016; Bertrand et al., 2016) suggests that it is likely primitive. The absence of this exposure in notharctines suggests greater expansion of the occipital lobes. As another reflection of the expansion of the temporal lobes, they are the widest part of the notharctine endocasts in dorsal view (Fig. 4), whereas the maximum width occurs closer to the occipital lobes in plesiadapiforms (Silcox et al., 2009b, 2010; Orliac et al., 2014). Expanded temporal and occipital lobes of the brain may be associated with visual specializations (Silcox et al., 2009b, 2010) based on a concentration of visual functions in those parts of the brain in living primates (i.e., see Barton, 2006: figure in box 4). In addition, the position of the rhinal sulcus is lower in the notharctine endocasts than that of plesiadapiforms, more similar to that of *A. parisiensis*, *R. viejaensis*, and *M. erinaceus* (Kirk et al., 2014; Ramdarshan and Orliac, 2015), suggesting that the neocortex was more developed in notharctines than in plesiadapiforms (Silcox et al., 2009b, 2010; Kirk et al., 2014; Orliac et al., 2014), which is consistent with measurements of neocortical area for euprimates compared to plesiadapiforms (Long et al., 2015). Neocortical surface area ratios calculated for specimens in this sample are reported in Table 5. Neocortical ratios calculated in this study of *N. tenebrosus* (0.31–0.33), *S. gracilis* (0.33–0.36), and *A. parisiensis* (0.33) are fairly similar and are consistently larger than those of plesiadapiforms reported in Long et al. (2015; 0.22–0.24). These details suggest that the brains of notharctines, like those of other known early euprimates, had relatively expanded neocortices, and the notharctines may have been more visually oriented than plesiadapiforms (Silcox et al., 2009b, 2010).

In contrast, the neocortical ratios of the adapiforms in this study were smaller than the ratios of *R. viejaensis* (0.44) and the omomyiform *M. erinaceus* (0.41; Ramdarshan and Orliac, 2015), suggesting that these species had relatively larger neocortices. Interestingly, the neocortical ratio of *A. parisiensis* obtained in this study (0.33) is smaller and more consistent with that of the other adapiforms than the neocortical ratio reported in Long et al. (2015; 0.43–0.53). Neocortical ratios of extant primates range from 0.60 to 0.81 (Long et al., 2015), suggesting that neither adapiforms nor omomyiforms had reached modern levels of neocorticalization (at least among sampled taxa).

5.2. Sylvian sulcus

Smilodectes gracilis had previously been noted as the only fossil or living euprimate known from endocasts to lack the Sylvian sulcus (Gazin, 1965; Radinsky, 1970; Gurche, 1978; Martin, 1990; Silcox

et al., 2010), a feature that has been suggested to be a defining derived characteristic of the euprimate brain (Elliot Smith, 1902; Martin, 1990). The condition of the Sylvian sulcus in *A. parisiensis* (Figs. 4 and 9) is comparable to that of modern primates and the Eocene euprimates *R. viejaensis*, *T. homunculus*, *N. antiquus*, and *M. erinaceus* (Radinsky, 1974; Gurche, 1982; Kirk et al., 2014; Ramdarshan and Orliac, 2015). Endocasts of *N. tenebrosus* show a shallow depression where a Sylvian sulcus is expected, but these depressions are not as defined as in *A. parisiensis*. Of the *S. gracilis* specimens in the sample, UM 32773 and USNM V 17996 do not exhibit any semblance of a fissure where a Sylvian sulcus would be expected. Images of USNM V 23276, the *S. gracilis* endocast described by Gazin (1965), also appear to lack a Sylvian sulcus. However, both USNM V 17994 and USNM V 21815 exhibit a shallow, but distinct Sylvian sulcus, thus revealing for the first time that at least some individuals of *S. gracilis* exhibited this otherwise ubiquitous euprimate trait.

The absence of the Sylvian sulcus in the endocasts of *S. gracilis* has been a source of much speculation (Martin, 1990). Absolute volume has a significant effect on the presence or absence of fissures on the brain, and many small-bodied mammals lack sulci, especially when brain mass is less than 5 g (Radinsky, 1975; Macrini et al., 2007). However, it is unlikely that small absolute brain volume is the main reason why many *S. gracilis* endocasts do not possess the feature, since *S. gracilis* brain volumes are all greater than 5 cm^3 and all other euprimate species represented by endocasts possess a Sylvian sulcus (Radinsky, 1970). This includes all fossil and modern euprimates with brain volumes absolutely smaller than that of *S. gracilis*, including those of *T. homunculus*, *R. viejaensis*, *Tarsius*, and *Microcebus murinus*. In addition, the absolute brain volumes of *N. tenebrosus* and *A. parisiensis* overlap with those of *S. gracilis* and a Sylvian sulcus is evident in all endocasts of the former species described in this study.

The level of compaction of the brain within the cranium is also thought to affect the formation of sulci (Mota and Herculano-Houzel, 2015), such that skull shape is another factor that can impact surface brain morphology (Martin, 1990). Radinsky (1970: p. 211) suggested that the Sylvian sulcus may have been absent in *S. gracilis* because it was a large-bodied primate with a larger skull and smaller orbits that "impinged less on the brain" than in other fossil primates such as *Tetonius*. Although *Smilodectes* does have less of a postorbital constriction than *A. parisiensis*, *N. tenebrosus* has a similar degree of postorbital constriction and preserves a Sylvian sulcus.

Another possibility is that the absence of the Sylvian sulcus in endocasts of *S. gracilis* may reveal the limitations of endocasts for representing brain morphology. Radinsky (1970) and Gurche (1982) suggested that subdural vessels could obscure the area around the Sylvian sulcus, hindering its preservation in endocasts. Gurche (1978) noted that the endocast of USNM V 23276 has faint, distinct ridges that could be traces of casts of vessels over the area of the Sylvian sulcus. Radinsky (1970: p. 211) did not identify any such ridges in USNM V 23276, but did report "two low, ventrally convergent, transverse ridges in the region where a Sylvian fissure would be expected to appear" on YPM 12125. The new endocasts of *S. gracilis* documented here provide some support for this hypothesis: all four of the virtual *S. gracilis* sample show faint ridges in the area of the Sylvian sulcus. Two *N. tenebrosus* endocasts (USNM V 23277 and 23278) exhibit similar raised ridges near the area of the Sylvian sulcus. These ridges are thicker on USNM V 23277 (SOM Fig. 3) and are finer and more numerous on USNM V 23278 (SOM Fig. 4). Given the relatively shallow Sylvian sulcus in *N. tenebrosus*, its absence on the majority of *S. gracilis* endocasts, and the evidence for subdural vessels presented herein, it is possible that the presence of obscuring vascular structures over the Sylvian sulcus is a common characteristic of notharctine endocasts. However, we doubt that this is a very likely possibility since endocasts of extant lemuriformes (even *Microcebus*) always show a close correspondence with the actual brain in preserving strong evidence of the Sylvian sulcus (unpublished endocasts generated by A. Harrington from scans published by Copes et al., 2016).

Even if the Sylvian sulcus was truly absent on the brains of *S. gracilis*, the significance of this feature is uncertain. One possibility is that *S. gracilis* retained the ancestral condition, as known plesiadapiforms do not possess a clear Sylvian sulcus either. Sylvian fossae are documented on the endocasts of *I. graybullianus* (Silcox et al., 2009b) and *P. tricuspidens* (Orliac et al., 2014), but not *M. annectens* (Silcox et al., 2010). However, these are much shallower than the Sylvian sulci of euprimates, and are also observed in *Tupaia* (Le Gros Clark, 1959). It is possible that the absence of a Sylvian sulcus in some specimens of *S. gracilis* is a retention of the ancestral condition. This could imply that the Sylvian sulcus evolved more than once, in separate lineages of euprimates.

5.3. Suprasylvian sulcus

Radinsky (1970) suggested that the presence of the suprasylvian sulcus (tentatively identified by Gazin, 1965) and absence of the Sylvian sulcus on *S. gracilis* (USNM 23276) were likely related. He proposed that as the orbits enlarge, they impinge on the brain and promote the formation of the Sylvian sulcus, which in turn may obscure the suprasylvian sulcus. No other known Eocene euprimate endocasts preserve the suprasylvian sulcus with the potential exception of *N. tenebrosus* (AMNH 127167), which has weakly developed Sylvian sulci. However, previous studies (Gazin, 1965; Radinsky, 1970; Gurche, 1978) have shown that the preservation of the suprasylvian sulcus is intraspecifically variable, so that the absence of the suprasylvian sulcus in *A. parisiensis*, *N. antiquus*, *T. homunculus*, *R. viejaensis*, and *M. erinaceus* may be an artifact of sample size. In plesiadapiforms, suprasylvian sulci have been identified in *M. annectens* and tentatively in *Plesiadapis cookei* and *Megadelphus ludeliusi* (Szalay, 1969; Gurche, 1978, 1982; Gingerich and Gunnell, 2005; Silcox et al., 2010). All of these plesiadapiforms lack a Sylvian sulcus (Silcox et al., 2010), which, combined with the presence of a tentative suprasylvian sulcus and the weak or absent Sylvian sulci in both *S. gracilis* and *N. tenebrosus*, lends support to Radinsky's (1970) hypothesis.

5.4. Cerebral proportions and sexual dimorphism

With the exception of the damaged USNM V 21815 endocast (Figs. 4 and 6), the cerebral proportions and appearance of the specimens of *S. gracilis* are quite similar to one another. In contrast, the proportions of the endocasts of *N. tenebrosus* are more variable (Figs. 4 and 6). It is possible that taphonomic distortion increased the variability of the *N. tenebrosus* sample, particularly with respect to AMNH 127167. While the maximum height to width ratios of USNM V 23277 and USNM V 23278 are identical, the lower ratio of AMNH 127167 may indicate the specimen experienced postmortem dorsoventral compression. However, fractures present in the AMNH 127167 cranium are minimal and concentrated in areas other than the braincase. The broken zygomatic arches of USNM V 23277 may indicate that the specimen experienced postmortem distortion, but there are no fractures in the braincase. In addition, the absolute height of USNM V 23277 is very similar to that of USNM V 23278, a specimen that seemingly has not been compressed laterally. In fact, the height to length ratio of USNM V 23278 is actually greater than in USNM V 23277. Given the apparently minimal postmortem distortion, it seems more likely that variation

in the endocast dimensions of *N. tenebrosus* reflects true biological variation in the species.

Similar to USNM V 23277, USNM V 21815 also has broken zygomatic arches and some potential evidence of taphonomic distortion in the lateral plane. Although the palate of this specimen of *S. gracilis* appears to be medio-laterally compressed (SOM Fig. 1L) and there is a dent on the side of the left parietal, there are no obvious cracks or breaks in the neurocranium to suggest significant overall dorsolateral compression of the resulting endocast. This suggests that the form of the endocast of USNM V 21815 also reflects a true biological variant. Interestingly, the two *S. gracilis* endocasts previously assigned to a sex (USNM V 17994, male and USNM V 21815, female; Alexander, 1994) differ in the same ways that AMNH 127167 (male) differs from the other *N. tenebrosus* endocasts. If previous sex attributions are correct, similarities in dorsoventral flatness (i.e., width:length ratio; see Fig. 6) of *N. tenebrosus* AMNH 127167 and all *S. gracilis* except USNM V 21815 may be reflective of them being males. As there is little morphological evidence of strong postmortem distortion in these crania, it seems likely that sexual dimorphism may be a causal factor for the observed variation in the notharctine endocasts. Though we identified USNM V 17996 as a female, based on the point of convergence of temporal lines, the specimen is fairly fragmentary, and the similarities of its endocranial shape to specimens more firmly identified as males suggest that this sex assignment may be incorrect.

It is unclear why the endocasts of the two species might vary with sex. Therefore, this idea must remain tentative until (1) this phenomenon can be documented in an extant taxon that can be considered to form an appropriate comparative model, and/or (2) better evidence can be accrued on sex assignment of notharctid individuals and bigger samples of specimens can be compared. If morphological traits used to diagnose sex are instead a reflection of intraspecific allometric variation, that could effectively explain similar patterns of observed variance in both species. However, the diagnostic features used to delineate males from females do not correlate with overall size of the individual. Therefore, at present, it is hard to imagine why canine size, detailed cranial features relating to sutural patterns, and brain morphology should correlate if they are not a reflection of sexual dimorphism. If we are wrong about dimorphism being the explanation for the observed variation in endocranial anatomy, then the observed correlations between shape (whether real or deformed) and morphology may be an artifact of the small sample size available.

5.5. Ontogeny and endocast morphology

Few studies have examined ontogenetic changes in endocast or brain morphology (but see Macrini et al., 2007). Since the cranium pertains to a juvenile, the brain of UM 32773 may still have been growing, but the amount of remaining growth is unclear. Despite its juvenility, the UM 32773 endocast is remarkably similar in appearance and proportion to the adult endocasts of USNM V 17994 and USNM V 17996, and has a greater absolute volume than the adult endocast of USNM V 21815. While UM 32773 has the greatest predicted body mass using the Dagosto and Terranova (1992) M^1 equation, its estimated EQ is only slightly less than that of USNM V 21815. With Dagosto and Terranova's (1992) M_1 equation, UM 32773 yields an EQ between USNM V 21815 and USNM V 17996. This suggests that UM 32773 had relatively little growth remaining before the brain reached adult size. This observation is consistent with data from modern *S. sciureus* (Franzen et al., 1990; Fig. 3), which show that most of the growth of the brain occurs very early in ontogeny in living primates. Indeed, based on the teeth that are erupted, if development in *S. gracilis* followed a similar trajectory, the brain of UM 32773 would be expected to be very near full adult brain mass (Fig. 3).

Body mass predictions derived from cranial lengths were not used in the calculation of EQ for UM 32773 because it is likely that they underpredict body mass for this specimen. Silcox et al. (2009a) reported a body mass of 629 g and 600 g using the vertical pGLS and horizontal pGLS cranial length equations, respectively. These values are up to about 50% lower than the cranially derived body masses for adult *S. gracilis* in this sample. When EQ is calculated for this specimen using these previously reported body masses from Silcox et al. (2009a), an EQ of 1.30 and 1.35 are obtained using the vertical pGLS and horizontal pGLS equations, respectively (see Fig. 10). This is above the range of EQs obtained for adults in the sample using either the vertical pGLS (0.74–0.95) or horizontal pGLS (0.65–0.87) equations. Because dentally-derived body masses for this specimen appear typical for this sample, this is further evidence that this individual of *S. gracilis* had not reached its full growth potential before death. Unfortunately, there are no postcrania of this specimen that may be useful for making further inferences about possible body mass at the time of death.

Morphologically, the UM 32773 endocast primarily differs from the adult specimens in its preservation of suture lines. Casts of the coronal, sagittal, and parietal-interparietal sutures are clearly visible on the endocast of UM 32773. A ridge along the coronal suture is visible on all the notharctine endocasts except for USNM V 17994, which Alexander (1994) has attributed to the tendency of the crania to separate along the coronal suture after death. This implies that the coronal suture is not obliterated in most adult crania of these notharctines. Based on illustrations by Gurche (1978, 1982), Endocast A, a partial natural endocast of *Notharctus*, also appears to preserve casts of the coronal and sagittal sutures, and potentially the parietal-interparietal suture. Unfortunately, Endocast A was not available for this study, but the preservation of suture lines on the endocast similar to UM 32773 suggests that this specimen was also from a juvenile.

5.6. Stratigraphy and endocast morphology

While this study presents the largest sample of endocasts of *N. tenebrosus* and *S. gracilis* yet available for analysis it is unlikely that a sample size of three for *N. tenebrosus* and four for *S. gracilis* captures the full picture of variation of brain morphology for these taxa. In addition to possible variation from sex or ontogeny, morphology of the brain in these fossil taxa may also have changed through time.

The *N. tenebrosus* endocasts examined here were found in localities in the Br2 biochron (Gunnell, 2002; Gunnell et al., 2008), which may span a million years (Robinson et al., 2004; see Fig. 1). Likewise, our *S. gracilis* endocasts are from localities from the Br2 and Br3 biochrons, which expands the temporal range of the sample to about 2 million years (Fig. 1). Gurche (1978) made the point that variation in the endocast morphology of fossil primates is not unexpected given the span of time in which a species existed. It is reasonable to expect significant variation among individuals from populations of disparate time periods, especially when comparable variation in brain morphology exists in concurrent populations (Gurche, 1978; Macrini et al., 2007).

While the locality where AMNH 127167 was collected is fairly precisely located (Alexander and Burger, 2001), the localities of the other two *N. tenebrosus* specimens are less so. However, two points of evidence support the inference that all of the *N. tenebrosus* specimens in this sample were likely found in the Br2 biochron. First, USNM V 23277 and USNM V 23278 were collected 10 miles east of Lyman, WY, and 0.5 miles south of Church Buttes, respectively, which are located within an area where the Br2 biochron is

exposed (Gunnell, 1998; Lay, n.d.). Furthermore, the specimens were collected in July–August 1959 during an expedition to Wyoming and Utah by C. Lewis Gazin, with a primary focus on collecting from Bridger B (=Br2 biochron) localities (Lay, n.d.; Dunkle, 1959). Presumably, it was during this same expedition that USNM V 23276, the specimen of *S. gracilis* described in Gazin (1965), was collected from a Br2 locality in or near section T 16 N, R 110 W, north of Cedar Mountain, which is southeast of Lyman, WY. In fact, field records indicate that USNM V 23277 was collected on August 4th, USNM V 23278 on August 9th, and USNM V 23276 on August 14th of that year, suggesting that they were collected as part of the same expedition, from the same beds.

The *S. gracilis* specimens appear to have come from more varied strata. UM 32773 was collected from a University of Michigan locality in the Br2 biochron. Similarly, USNM V 17996 was found near Pinnacle Rock, located in the Br2 biochron. USNM V 21815 is also recorded to be a Bridger B (=Br2) specimen. However, USNM V 17994 was noted in the original collection tag to have been located in the Bridger C from a locality on Twin Buttes, which corresponds to the Br3 biochron.

While the skulls used in this study may thus be confined to particular Bridgerian biochrons, no more precise dating or stratigraphic information exist. It is interesting that the *S. gracilis* endocast from the Br3 layer, USNM V 17994, is quite similar to the other undamaged *S. gracilis* endocasts under discussion, although it seems to be the only specimen separated in time. Thus, to the extent that there are data available that can speak to the question, stratigraphic differences do not help explain the variation in the virtual endocasts described here.

5.7. *Was* S. gracilis *more encephalized than* N. tenebrosus*?*

Body mass predictions calculated from dental equations in this study (Fig. 10 and Table 6) would indicate that individuals of *N. tenebrosus* in the sample had a greater body mass than those of *S. gracilis*. The apparent difference in body mass between these two species is particularly pronounced when comparing the predictions of the all-primate Gingerich et al. (1982) M^1 equation. In contrast, cranial length equations yield more similar body masses for sampled individuals of the two species although the range of variation is still shifted downward for *S. gracilis* relative to *N. tenebrosus* (Fig. 10A). Body masses derived from cranial length are consistently lower than those predicted using all dental proxies. This would suggest that some change has occurred in the relative scaling of teeth and/or crania to body mass through evolutionary time, making one (or both) of these proxies problematic as a source of body mass prediction using equations based on samples of modern primates.

As teeth and crania are not weight-bearing structures, postcranial proxies may be better predictors of body mass (Hylander, 1980; Gingerich, 1990; Yapuncich et al., 2015). Problematically, no single postcranial element has been preserved with all of the specimens in this sample, so means of the articular surface area of the astragalar ectal facet (EFA) were used to predict body masses. The results of this last body mass prediction method are consistent with the idea that the body masses of *N. tenebrosus* and *S. gracilis* overlapped, although the species mean mass of *N. tenebrosus* was slightly larger than that of *S. gracilis* (2902 g vs. 2595 g; Table 6). For *S. gracilis*, the EFA prediction was closest in value to the body mass predictions of the Gingerich et al. (1982) M^1 equation, while in *N. tenebrosus*, it was closest in value to the body mass predictions that resulted using the Dagosto and Terranova (1992) M^1 equations.

Assessing which body mass prediction equations yield the most accurate predictions for these two species is a difficult matter to resolve. On the one hand, equations using M^1 metrics may be favored as each individual in the sample preserves this feature, and it is effectively the only body mass proxy available for direct specimen-to-specimen comparisons. However, whether the all-primate M^1 (Gingerich et al., 1982) or the strepsirrhine-only M^1 (Dagosto and Terranova, 1992) equation is more appropriate is open to debate. If adapiforms are stem strepsirrhines (Gregory, 1920; Beard et al., 1986; Martin, 1990; Kay et al., 1997; Williams et al., 2010a,b; Maiolino et al., 2012) it might seem more appropriate to use the Dagosto and Terranova (1992) equations because they were generated with a strepsirrhine-only reference sample. However, even if this phylogenetic hypothesis is true, it is still not clear that stem strepsirrhines would have followed the same scaling rules as members of the crown primates. Yapuncich et al. (2015) demonstrated that while the mean percentage prediction error (%MPE) of the Gingerich et al. (1982) equation is quite high (~47%), the %MPEs of both the M^1 and M_1 equations of the Dagosto and Terranova (1992) equations were ~44%, which indicates that the latter equations were only slightly more reliable. In addition, the PRESS (prediction sum of squares; Allen, 1974; Smith, 2002) statistics calculated for this study (SOM Table 2) indicate that the PRESS RMSE (root mean square prediction error) is highest (0.509) for the Dagosto and Terranova (1992) M^1 equation among all of the body mass prediction equations used in this study, indicating that this equation may be slightly less reliable than the Gingerich et al. (1982) M^1 equation (0.460) and the Dagosto and Terranova (1992) M_1 equation (0.388).

Of the cranial length body mass prediction equations, the vertical pGLS equation is preferred since *N. tenebrosus* and *S. gracilis* likely habitually used vertical postures (Gebo, 1988; Schmitt, 1996; Silcox et al., 2009a). Body mass predictions using cranial length as a proxy are also advantageous in that the EQ estimates may be made using body masses predicted for individuals in the sample. While the MPEs of the cranial equations have not been assessed and cannot be used to compare to the dental equations, PRESS statistics of the two cranial length equations from Silcox et al. (2009a) yield the lowest PRESS RMSEs. Unfortunately, for all specimens in the sample except USNM V 21815, full prosthion–inion lengths could not be measured due to the incomplete preservation of the crania, particularly of their premaxillae. Thus, the measurements of cranial length are not strictly comparable across all specimens. Additionally, no correction factors were applied to the cranial length equations, so that predicted body masses are likely to be systematically under predicted when they were de-transformed from the logarithmic scale (Smith, 1993).

The use of EFA as a predictor of body mass is advantageous because of the weight-bearing nature of the facet. This tarsal body mass prediction equation has also been demonstrated to be more precise ($r^2 = 0.96$) and more accurate (MPE = 27%) than the dental equations used in this study (Yapuncich et al., 2015), and is more precise than the cranial length body mass prediction equations based on coefficients of determination. The reference sample for the equation also spans a much broader taxonomic range than any of the other prediction equations. However, direct specimen-to-specimen comparison is impossible within the sample and the use of averages from unassociated postcrania may be problematic due to potential intraspecific variation between individuals, as well as through time and across geography. The PRESS RMSE of the EFA prediction equation (0.33) is higher than the cranial length equations, but slightly lower than all dental equations, indicating the tarsal equation may only be slightly more reliable than the dental equations.

It is notable that in the only specimen of the endocast sample in which the astragalus is preserved (USNM V 17994), the EFA predicts a body mass (2849 g) that is most similar to the one predicted for it by the Gingerich et al. (1982) M^1 equation. This might suggest that

the Gingerich et al. (1982) M^1 is the best proxy for body mass prediction when postcrania are absent for the individual specimens. Yet this is problematic because the EFA and cranial length body mass predictions both suggest that the body masses of *N. tenebrosus* and *S. gracilis* are similar. If cranial length and EFA are more reliable proxies for predicting body mass than the dental measurements, which the PRESS RMSE values suggest, the differences in predicted body mass suggest that *N. tenebrosus* was megadont, with relatively large molars for its body size, and the Gingerich et al. (1982) equation is less applicable to that species than to *S. gracilis*. In further support of the idea that crania and postcrania (rather than teeth) are presenting a more accurate picture of the relative size of *S. gracilis* and *N. tenebrosus* are results of MacLarnon (1996) using data on femoral cross section. She shows nearly identical femur-based estimates of *S. gracilis* (average body mass was 2641 g for $n = 5$ specimens) and *N. tenebrosus* (average body mass was 2695 g for $n = 3$ specimens). These predictions are also surprisingly close to the values suggested by EFA. Recovery of *N. tenebrosus* specimens that preserve dental elements in association with an astragalus could allow this hypothesis to be tested.

Results of this study suggest that, on average, *S. gracilis* had higher EQs than *N. tenebrosus*. No matter which regression is used, when the individual specimens in the sample are averaged, the mean EQ of *S. gracilis* is somewhat higher (in the case of EFA and cranial body mass prediction equations) and markedly higher (in the case of dental predictions; see Fig. 10B and Table 6) than those of *N. tenebrosus*.

5.8. Implications of early euprimate EQs

Different EQs of *N. tenebrosus* and *S. gracilis* might suggest ecological or behavioral differences that generated varying selective pressures on brain size. Differences in diet, visual specializations, and social structure are hypothesized to affect the level of encephalization in Primates (Harvey et al., 1980; Barton, 2004; Kirk, 2006; Dunbar and Shultz, 2007; Silcox et al., 2010). Among small-bodied mammals and primates, folivores are relatively less encephalized compared to closely related non-folivorous taxa (Harvey et al., 1980). Based on dental characteristics and analyses, *N. tenebrosus* and *S. gracilis* have both been suggested to be folivorous (Covert, 1986, 1995; Gilbert, 2005; Sauther and Cuozzo, 2012; Fleagle, 2013). However, if *N. tenebrosus* was megadont, then its larger teeth may reflect a more folivorous diet (Kay, 1975; Anthony and Kay, 1993; Boyer et al., 2010; Winchester et al., 2014).

The social brain hypothesis posits that primate brains expanded along with the evolution of intricate social systems as measured by group size (Dunbar and Shultz, 2007). Among modern primates, there is a positive relationship between relative brain size and sociality (Dunbar and Shultz, 2007), and the increase in primate brain size relative to other mammals may have been caused by changes in social behavior (Shultz and Dunbar, 2010). Unfortunately, social behavior is difficult to infer in extinct animals, but the observed sexual dimorphism in *N. tenebrosus* and *S. gracilis* may indicate some degree of male–male competition and a polygynous mating system (Plavcan, 2000, 2004). *Notharctus tenebrosus* specimens exhibit more canine and craniofacial sexual dimorphism than *S. gracilis* specimens (Alexander, 1994), suggesting sexual selection was more pronounced in the former species. Recent studies (Schillaci, 2006, 2008) have shown that monogamous primates have relatively larger brains and neocortices than non-monogamous species with intense male–male competition (particularly among hominoids). If reduced EQs are indeed associated with strong intrasexual selection, the pattern could explain the reduced EQs in *N. tenebrosus* compared to the less dimorphic *S. gracilis*. However, fossils do not preserve sufficient information to infer group size and/or other proxies for the degree of social complexity, making it difficult to test the social brain hypothesis in extinct species.

5.9. How encephalized were notharctines relative to other primates?

Regardless of the body mass prediction equation used, it is unlikely that *N. tenebrosus* and *S. gracilis* were as encephalized as extant primates. This might not be surprising if notharctines are, in fact, stem strepsirrhines, branching off early in the group's evolution. This contrast is reflected in the indications of less cerebral expansion evident on the notharctine endocasts (e.g., narrow frontal lobes, lack of overlap on the olfactory bulbs) and lower neocortical ratios relative to extant primates. Lower EQs for notharctines suggest they were not much more encephalized than some plesiadapiforms (e.g., *I. graybullianus* and *M. annectens*). However, the higher neocortical ratios, expanded temporal and occipital lobes, and relatively smaller olfactory bulbs of the notharctines reinforce previous studies suggesting that the earliest euprimates were more reliant on vision than olfaction compared to plesiadapiforms (Silcox et al., 2009b, 2010).

This observation is quite intriguing as it parallels an apparently common trend in primate brain evolution. Specifically, the Fayum catarrhine *Aegyptopithecus* (Simons et al., 2007), while having a strepsirrhine-like EQ, was described as exhibiting a more advanced brain morphology. More recently, the basal cercopithecoid *Victoriapithecus* (Gonzales et al., 2015) was shown to have evolved morphologically distinctive cercopithecoid endocast while retaining a very low EQ. This may suggest that as new structures evolve in the brain in association with enhanced sensory capacities or configurations, selection for brain enlargement follows to achieve more complex executive functions that can effectively utilize those improved sensory capabilities.

Interestingly, depending on the body mass prediction proxy used, the level of encephalization of the adapiforms in this sample changes relative to non-adapiform early euprimates (e.g., *R. viejaensis* and *M. erinaceus*). In particular, the EQ of *M. erinaceus* predicted by the Martin (1990) cranial length equation is well within the range of extant strepsirrhines, but when the Gingerich et al. (1982) M^1 equation is used, the EQ is comparable to the EQ of *S. gracilis* using this same proxy (Fig. 11). This could suggest megadonty in *M. erinaceus* and *R. viejaensis* relative to their skull length, or suggest that the cranial lengths of these two species are relatively short for their body mass if the dental and postcranial predictions are a more accurate measure of their body mass. This could also indicate that the encephalization quotients of the two non-adapiform early euprimates overlap with those of the most encephalized adapiforms in our sample, despite the seemingly more derived traits of the former's endocasts: overlap of the cerebellum over occipital lobe, smaller olfactory bulbs, and larger neocortical ratios.

5.10. Summary and conclusions

This study documents the first virtual endocasts of the notharctine primates *N. tenebrosus* and *S. gracilis*, increasing the sample size of endocasts that may be evaluated and quantitatively compared. Relative to previous studies of these early Eocene primates, volumes could be measured with fewer sources of error. Also, surface morphology could be visualized at a higher resolution, and the sample size of specimens available for study was expanded due to the non-destructive technique of endocast extraction.

The endocranial morphology of *N. tenebrosus* is consistent in many ways with that of *S. gracilis* and the adapine adapiform *A. parisiensis*. All three species have small frontal lobes relative to extant primates, a cerebrum which does not overlap onto

the olfactory bulbs or cerebellum, and smaller olfactory bulbs and more expanded temporal and occipital lobes compared to plesiadapiforms. Natural endocasts of *S. gracilis* have been known for some 50 years, and virtual endocasts documented in this study are broadly consistent with previous findings. However, USNM V 17994 and USNM V 21815 preserve indications of the first Sylvian sulci known in *S. gracilis*, indicating that at least some members of this species did possess this distinctive euprimate trait. Vasculature located around the area of the Sylvian sulcus may obscure the presence of this feature in other specimens of *S. gracilis*, as originally suggested by Radinsky (1970).

While the range of variation is similar when considering the extremes in both the *N. tenebrosus* and *S. gracilis* samples, there is more uniformity in the *S. gracilis* sample since 75% of the *S. gracilis* are more similar to each other in the relative proportions of the endocast, while only 66% of *N. tenebrosus* are. Among the *N. tenebrosus* sample, the virtual endocast of AMNH 127167 exhibits a more *S. gracilis*-like dorsal outline (i.e., in being more globular), USNM V 23277 has a more *A. parisiensis*-like outline (i.e., more rostro-caudally elongate, less globular), while USNM V 23278 may be described as intermediate. The greater variability in *N. tenebrosus* was not expected, as the three skulls are likely to be from a shorter temporal interval than the *S. gracilis* sample. Additionally, all *N. tenebrosus* specimens in the sample were adults, while UM 32773 represents a juvenile *S. gracilis* specimen that nonetheless presents surface morphology and proportions very similar to the adult *S. gracilis* endocasts (except USNM V 21815). The brains of *N. tenebrosus* may have been more variable in surface morphology, volume, and proportions than *S. gracilis*, but small sample sizes preclude robust statistical analyses. Currently, sexual dimorphism (based on previous identification of AMNH 127167 as male, USNM V 17994 as male, USNM V 21815 as female, and USNM V 23277-78 as female based on canine size) correlates best with observed variation in brain morphology, but this observation must be tested with greater sampling.

Because the range of endocranial volumes for *N. tenebrosus* and *S. gracilis* overlap, any difference in their degree of encephalization will be the result of differing body mass predictions. The only predictor variable preserved in all specimens of the sample was M^1 occlusal area – although cranial lengths are reported for all specimens, this measure could not be standardized due to variable preservation of the premaxilla. Encephalization quotient estimates based on body masses from M^1 regressions (Gingerich et al., 1982; Dagosto and Terranova, 1992) suggest *N. tenebrosus* was less encephalized than *S. gracilis*, although future studies should investigate the possibility of megadonty in *N. tenebrosus*. Cranial and tarsal body mass prediction equations both suggest the EQs of these two species overlapped, but on average, *S. gracilis* appeared to be more encephalized than *N. tenebrosus*.

Overall, *N. tenebrosus* and *S. gracilis* appear to have been less encephalized than any extant primate. In fact, this study suggests that the relative encephalization of adapiforms may have not been much greater than that of plesiadapiforms. Nonetheless, there is evidence that the brains of these early euprimates were becoming more like those of later euprimates in structure even if relative volume may not have increased tremendously in the direction of extant euprimates. The higher neocortical ratios, smaller percentage of the olfactory bulb to brain volume and body size, and expansion of the temporal and occipital lobes suggest that early euprimates were becoming more reliant on vision and less reliant on olfaction than plesiadapiforms. These differences in the structure of plesiadapiform and adapiform endocasts could suggest that some key characteristics that define extant euprimates developed before marked increase in brain volume occurred during the evolutionary history of the lineage.

Acknowledgments

We would like to thank Dr. Timothy Ryan and Tim Stecko of the Center for Quantitative X-ray Imaging at Pennsylvania State University for performing the CT scan of AMNH 127167, and Dr. Jin Meng and Carl Mehling of the American Museum of Natural History for facilitating the loan of AMNH 127167, Dr. Nicholas Pyenson and David Bohaskas for facilitating the loan of specimens from the Smithsonian Insitution, Dr. Gregg Gunnell for providing dental measurements and locality information for UM 32773, and GSY would like to thank Dr. Marian Dagosto for kindly providing raw data from Dagosto and Terranova (1992) in order to calculate PRESS and prediction intervals for those equations. Research was funded in part by the Florida Museum of Natural History, a Faculty Enhancement Opportunity (FEO) award from the University of Florida (to J. Bloch), the National Science Foundation (EF-0629836 to J. Bloch, M. Silcox, and E. Sargis, BCS 1440742 to D. Boyer and G. Gunnell, and BSC 144558 to J. Bloch), and the Natural Sciences and Engineering Research Council of Canada (to M. Silcox).

Supplementary Online Material

Supplementary online material related to this article can be found at http://dx.doi.org/10.1016/j.jhevol.2016.06.005.

References

Alexander, J.P., 1994. Sexual dimorphism in notharctid primates. Folia Primatol. 63, 59–62.
Alexander, J.P., Burger, B.J., 2001. Stratigraphy and taphonomy of Grizzly Buttes, Bridger formation, and the middle Eocene of Wyoming. In: Gunnell, G.F. (Ed.), Eocene Biodiversity: Unusual Occurrences and Rarely Sampled Habitats. Plenum Press, New York, pp. 165–196.
Allen, D.M., 1974. The relationship between variable selection and data augmentation and a method for prediction. Technometrics 16, 125–127.
Anthony, M.R., Kay, R.F., 1993. Tooth form and diet in ateline and alouattine primates: reflections on the comparative method. Am. J. Sci. 293-A, 356–382.
Barton, R.A., 2004. Binocularity and brain evolution in primates. Proc. Natl. Acad. Sci. 101, 10113–10115.
Barton, R.A., 2006. Primate brain evolution: integrating comparative, neurophysiological, and ethological data. Evol. Anthropol. 15, 224–236.
Beard, K.C., Dagosto, M., Gebo, D.L., Godinot, M., 1986. Interrelationships among primate higher taxa. Nature 331, 712–714.
Beard, K.C., 1988. New notharctine primate fossils from the early Eocene of New Mexico and southern Wyoming and the phylogeny of Notharctinae. Am. J. Phys. Anthropol. 75, 439–469.
Bertrand, O.C., Silcox, M.T., 2016. First virtual endocasts of a fossil rodent: *Ischyromys typus* (Ischyromyidae) and brain evolution in rodents. J. Vert. Paleontol. http://dx.doi.org/10.1080/02724634.2016.1096275.
Bertrand, O.C., Amador-Mughal, F., Silcox, M.T., 2016. Virtual endocasts of *Paramys* (Paramyinae): oldest endocranial record for Rodentia and early brain evolution in Euarchontoglires. Proc. R. Soc. B 283. http://dx.doi.org/10.1098/rspb.2015.2316, 20152316.
Bloch, J.I., Silcox, M.T., Boyer, D.M., Sargis, E.J., 2007. New Paleocene skeletons and the relationship of plesiadapiforms to crown-clade primates. Proc. Natl. Acad. Sci. 104, 1159–1164.
Boyer, D.M., Seiffert, E.R., 2013. Patterns of astragalar fibular facet orientation in extant and extinct primates and their evolutionary implications. Am. J. Phys. Anthropol. 151, 420–447.
Boyer, D.M., Evans, A., Jernvall, J., 2010. Evidence of dietary differentiation among late Paleocene-early Eocene plesiadapids (Mammalia, Primates). Am. J. Phys. Anthropol. 142, 194–210.
Boyer, D.M., Seiffert, E.R., Gladman, J.T., Bloch, J.I., 2013a. Evolution and allometry of calcaneal elongation in living and extinct primates. PLoS One 8, e67792.
Boyer, D.M., Yapuncich, G.S., Chester, S.G.B., Bloch, J.I., Godinot, M., 2013b. Hands of early primates. Am. J. Phys. Anthropol. 57, 33–78.
Boyer, D.M., Yapuncich, G.S., Butler, J.E., Dunn, R.H., Seiffert, E.R., 2015. Evolution of postural diversity in primates as reflected by the size and shape of the medial tibial facet of the talus. Am. J. Phys. Anthropol. 157, 134–177.
Boyer, D.M., Gunnell, G.F., Kaufman, S., McGeary, T., 2016. MorphoSource – Archiving and Sharing Digital Specimen Data. J. Paleontol. (in press).
Cartmill, M., 1992. New views on primate origins. Evol. Anthropol. 1, 105–111.
Conroy, G.C., 1987. Problems in body-weight estimation in fossil primates. Int. J. Primatol. 8, 115–137.

Copes, L.E., Lucas, L.M., Thostenson, J.O., Hoesktra, H.E., Boyer, D.M., 2016. A collection of non-human primate computed tomography scans housed in MorphoSource, a repository for 3D data. Sci. Data 3, 160001.
Covert, H.H., 1986. The biology of early Cenozoic primates. In: Swindler, D.R., Erwin, J. (Eds.), Comparative Primate Biology, Systematics, Evolution, and Anatomy, vol. 1. Alan R. Liss, New York, pp. 335–359.
Covert, H.H., 1990. Phylogenetic relationships among the Notharctinae of North America. Am. J. Phys. Anthropol. 81, 381–397.
Covert, H.H., 1995. Locomotor adaptations of Eocene primates: adaptive diversity among the earliest prosimians. In: Alterman, L., Doyle, G.A., Izard, M.K. (Eds.), Creatures of the Dark: The Nocturnal Prosimians. Plenum Press, New York, pp. 495–509.
Clutton-Brock, T.H., Harvey, P.H., 1980. Primates, brain, and ecology. J. Zool., Lond. 190, 309–323.
Clyde, W.C., Zonnveld, J.-P., Stametakos, J., Gunnell, G.F., Bartels, W.S., 1997. Magnetostratigraphy across the Wasatchian-Bridgerian (early to middle Eocene) in the western Green River Basin. Wyoming. J. Geol. 105, 657–669.
Clyde, W.C., Sheldon, N.D., Koch, P.L., Gunnell, G.F., Bartels, W.S., 2001. Linking the Wasatchian/Bridgerian boundary to the Cenozoic global climate optimum: new magnetostratigraphic and isotopic results from South Pass. Wyoming. Palaeogeogr. Palaeoclimatol. Palaeoecol. 167, 175–199.
Dagosto, M., Terranova, C.J., 1992. Estimating the body size of Eocene primates: a comparison of results from dental and postcranial variables. Int. J. Primatol. 13, 307–344.
Dunbar, R.I.M., 1998. The social brain hypothesis. Evol. Anthropol. 6, 178–190.
Dunbar, R.I.M., Shultz, S., 2007. Understanding primate brain evolution. Phil. Trans. R. Soc. B 362, 649–658.
Dunkle, D.H., 1959. U.S. National Museum. Sc. Vert. Paleo. News Bull. 56, 11.
Eisenberg, J.F., 1981. The Mammalian Radiations: an Analysis of the Trends in Evolution, Adaptation, and Behavior. University of Chicago Press, Chicago and London.
Edinger, Tilly, 1964. Midbrain exposure and overlap in mammals. Am. Zool. 1, 5–19.
Elliot Smith, G., 1902. On the morphology of the brain in Mammalia, with special reference to that of lemurs, recent and extinct. Trans. Linn. Soc. Lond. (Zool.) 8, 319–432.
Fleagle, J.G., 2013. Primate Adaptation and Evolution. Academic Press, New York.
Franzen, J.L., Gingerich, P.D., Habersetzer, J., Hurum, J.H., von Koenigswald, W., Smith, B.H., 2009. Complete primate skeleton from the middle Eocene of Messel in Germany: Morphology and Paleobiology. PLoS One 4, 1–27.
Gazin, C.L., 1958. A review of the Middle and Upper Eocene primates of North America (with 14 Plates). Smithsonian Misc. Coll. 136, 1–116.
Gazin, C.L., 1965. An endocranial cast of the Bridger Middle Eocene primate *Smilodectes gracilis*. Smithsonian Misc. Coll. 149, 1–14.
Gebo, D.L., 1988. Foot morphology and locomotor adaptation in Eocene primates. Folia Primatol. 50, 3–41.
Gebo, D.L., 2002. Adapiformes: phylogeny and adaptation. In: Hartwig, W.C. (Ed.), The Primate Fossil Record. Cambridge University Press, Cambridge, pp. 21–44.
Gilbert, C.C., 2005. Dietary ecospace and the diversity of euprimates during the Early and Middle Eocene. Am. J. Phys. Anthropol. 126, 237–249.
Gingerich, P.D., 1976. Cranial anatomy and evolution of early Tertiary Plesiadapidae (Mammalia, Primates). U. Mich. Pap. Paleo. 15, 1–140.
Gingerich, P.D., 1980. Eocene Adapidae, paleobiogeography, and the origin of South American Platyrrhini. In: Cichon, R.L., Chiarelli, A.B. (Eds.), Evolutionary Biology of the New World Monkeys and Continental Drift. Plenum, New York, pp. 123–138.
Gingerich, P.D., 1981. Cranial morphology and adaptations in Eocene Adapidae I: Sexual dimorphism in *Adapis magnus* and *Adapis parisiensis*. Am. J. Phys. Anthropol. 56, 217–234.
Gingerich, P.D., 1990. Prediction of body mass in mammalian species from long bone lengths and diameters. Contrib. Mus. Paleontol. Univ. Mich. 28, 79–92.
Gingerich, P.D., Gunnell, G.F., 2005. Brain of *Plesiadapis cookei* (Mammalia, Proprimates): surface morphology and encephalization compared to those of Primates and Dermoptera. Contrib. Mus. Paleontol. Univ. Mich. 31, 185–195.
Gingerich, P.D., Martin, R.D., 1981. Cranial morphology and adaptations in Eocene Adapidae II: the Cambridge skull of *Adapis parisiensis*. Am. J. Phys. Anthropol. 56, 235–257.
Gingerich, P.D., Smith, B.H., 2010. Premolar development and eruption in the early Eocene adapoids *Cantius ralstoni* and *Cantius abditus* (Mammalia, Primates). Contrib. Mus. Paleontol. Univ. Mich. 32, 41–47.
Gingerich, P.D., Smith, B.H., Rosenberg, K.R., 1982. Allometric scaling in the dentition of primates and prediction of body weight from tooth size in fossils. Am. J. Phys. Anthropol. 58, 81–100.
Gingerich, P.D., Franzen, J.L., Habersetzer, J., Hurum, J.H., Smith, B.H., 2010. *Darwinius masillae* is a haplorhine—reply to Williams et al. (2010). J. Hum. Evol. 59, 574–579.
Gonzales, L.A., Benefit, B.R., McCrossin, M.L., Spoor, F., 2015. Cerebral complexity preceded enlarged brain size and reduced olfactory bulbs in Old World Monkeys.Nature Comm. 6: 7580, 1–9.
Gregory, W.K., 1920. On the structure and relations of *Notharctus*, an American Eocene primate. Mem. Am. Mus. Nat. Hist. 3, 49–243.
Gunnell, G.F., 1995. New Notharctinae (Primates, Adapiformes) skull from the Uintan (Middle Eocene) of San Diego County, California. Am. J. Phys. Anthropol. 98, 447–470.
Gunnell, G.F., 1998. Mammalian fauna from the lower Bridger Formation (Bridger A, early middle Eocene) of the southern Green River Basin, Wyoming. Contrib. Mus. Paleontol. Univ. Mich. 30, 83–130.
Gunnell, G.F., 2002. Notharctine primates (Adapiformes) from the early to middle Eocene (Wasatchian-Bridgerian) of Wyoming: transitional species and the origins of *Notharctus* and *Smilodectes*. J. Hum. Evol. 43, 353–380.
Gunnell, G.F., Rose, K.D., 2002. Tarsiiformes: evolutionary history and adaptation. In: Hartwig, W.C. (Ed.), The Primate Fossil Record. Cambridge University Press, Cambridge, pp. 45–82.
Gunnell, G.F., Rose, K.D., Rasmussen, D.T., 2008. Euprimates. In: Janis, C., Gunnell, G.F., Uhen, M.D. (Eds.), Evolution of Tertiary Mammals in North America, Small Mammals, Xenarthrans, and Marine Mammals, volume 2. Cambridge University Press, New York, pp. 239–261.
Gunnell, G.F., Murphey, P.C., Stucky, R.K., Townshend, K.E.B., Robinson, P., Zonneveld, J.P., Bartels, W.S., 2009. Biostratigraphy and biochronology of the latest Wasatchian, Bridgerian, and Uintan North American land mammal "ages". In: Albright, L.B. (Ed.), Papers on Geology, Vertebrate Paleontology, and Biostratigraphy in Honor of Michael O. Woodburne, Mus. N. Ariz. Bull., 65, pp. 279–330.
Gurche, J.A., 1978. Early primate brain evolution. Master's thesis, University of Kansas.
Gurche, J.A., 1982. Early primate brain evolution. In: Armstrong, E., Falk, D. (Eds.), Primate Brain Evolution: Methods and Concepts. Plenum, New York, pp. 227–246.
Hamrick, M.W., Alexander, J.P., 1996. The hand skeleton of *Notharctus tenebrosus* (Primates, Notharctidae) and its significance for the origin of the primate hand. Am. Mus. Novit. 3182, 1–20.
Harvey, P.H., Clutton-Brock, T.H., Mace, G.M., 1980. Brain size and ecology in small mammals and primates. Proc. Natl. Acad. Sci. 77, 4387–4389.
Healy, S.D., Rowe, C., 2007. A critique of comparative studies of brain size. Proc. R. Soc. B. 274, 453–464.
Heritage, S., 2014. Modeling olfactory bulb evolution through primate phylogeny. PLoS One 9, e113904.
Hofer, H.O., 1962. Über die interpretation der ältesten fossilen primatengehirne. Bibliogr. Primatol. 5, 1–31.
Hofer, H.O., Wilson, J.A., 1967. An endocranial cast of an early Oligocene primate. Folia Primatol. 5, 148–152.
Hoffstetter, R., 1977. Phylogenie des primates. Bulletins et Memoires de la Societe d'Anthropolgie de Paris t. 4, serie XIII 327–346.
Hürzeler, J., 1948. Zur Stammegeschichte der Necrolemuriden. Schweiz. Palaont. Abh. 66, 3–46.
Hylander, W.L., 1980. Mandibular function and biomechanical stress and scaling. Am. Zool. 159, 253–296.
Isler, K., Kirk, C.E., Miller, J.M.A., Albrecht, G.A., Gelvin, B.R., Martin, R.D., 2008. Endocranial volumes of primate species: scaling analyses using a comprehensive and reliable data set. J. Hum. Evol. 55, 967–978.
Jerison, H.J., 1973. Evolution of the Brain and Intelligence. Academic Press, New York.
Jerison, H.J., 1979. Brain, body, and encephalization in early primates. J. Hum. Evol. 8, 615–635.
Jerison, H.J., 2007. Fossils, brains, and behavior. In: Watanabe, S., Hoffman, M.A. (Eds.), Integration of Comparative Neuroanatomy and Cognition. Keio University Press, Tokyo, pp. 13–31.
Jerison, H.J., 2012. Digitized fossil brains: neocorticalization. Biolinguistics 6, 383–392.
Kay, R.F., 1975. The functional adaptations of primate molar teeth. Am. J. Phys. Anthropol. 43, 195–215.
Kay, R.F., Ross, C., Williams, B.A., 1997. Anthropoid origins. Science 275, 797–804.
Kirk, E.C., 2006. Visual influences on primate encephalization. J. Hum. Evol. 51, 76–90.
Kirk, E.C., Daghighi, P., Macrini, T.E., Bhullar, B.A.S., Rowe, T.B., 2014. Cranial anatomy of the Duchesnean primate *Rooneyia viejaensis*: new insights from high resolution computed tomography. J. Hum. Evol. 74, 82–95.
Lay, M., n.d. Fossil collecting expeditions led by the division of vertebrate paleontology during the 1950s. http://paleobiology.si.edu/history/lay1950s.html.
Le Gros Clark, W.E., 1945. Note on the paleontology of the lemuroid brain. J. Anat. 79, 123–126.
Le Gros Clark, W.E., 1959. The Antecedents of Man. Edinburgh University Press, Edinburgh.
Long, A., Bloch, J.I., Silcox, M.T., 2015. Quantification of neocortical ratios in stem primates. Am. J. Phys. Anthropol. 157, 363–373.
Long, J.O., Cooper, R.W., 1968. Physical growth and dental eruption in captive-bred squirrel monkeys, *Saimiri sciureus* (Leticia, Columbia). In: Rosenblum, L., Cooper, R. (Eds.), The Squirrel Monkey. Academic Press, New York and London, pp. 169–205.
López Torres, S., Schillaci, M.A., Silcox, M.T., 2015. Life history of the most complete fossil primate skeleton: exploring growth models for *Darwinius*. Royal. Soc. Open Sci. 2, 150340.
MacLarnon, A., 1996. The evolution of the spinal cord in primates: Evidence from the foramen magnum and the vertebral canal. J. Hum. Evol. 30, 121–138.

Macrini, T.E., Rowe, T., VandeBerg, J.L., 2007. Cranial endocasts from a growth series of *Monodeplphis domestica* (Didelphidae, Marsupialia): a study of individual and ontogenetic variation. J. Morphol. 268, 844–865.
Maiolino, S., Boyer, D.M., Bloch, J.I., Gilbert, C.C., Groenke, J., 2012. Evidence for a grooming claw in a North American adapiform primate: implications for anthropoid origins. PLoS One 7, 1–28.
Manocha, S.L., 1979. Physical growth and brain development of captive-bred male and female squirrel monkeys, *Saimiri sciureus*. Experientia 35, 96–98.
Martin, R.D., 1990. Primate Origins and Evolution: a Phylogenetic Reconstruction. Chapman and Hall, London.
Montgomery, S.H., Capellini, I., Barton, R.A., Mundy, N.I., 2010. Reconstructing the ups and downs of primate brain evolution: implications for adaptive hypotheses and *Homo floresiensis*. BMC Biol. 8, 9.
Mota, B., Herculano-Houzel, S., 2015. Cortical folding scales universally with surface area and thickness, not number of neurons. Science 349, 74–77.
Murphey, P.C., Lester, A., Bohor, B., Robinson, P., Evanoff, E., Larson, E., 1999. $^{40}Ar/^{39}Ar$ dating of volcanic ash deposits in the Bridger Formation (middle Eocene), southwestern Wyoming. Geol. Soc. Am. Abstracts with Programs 33, A-233.
Neumayer, L., 1906. Ueber das Gehirn von *Adapis parisiensis* Cuv. Cuv. Neues. Jahrb. Min. Geol. Palaont. 2, 100–104.
O'Leary, M.A., Bloch, J.I., Flyinn, J.J., Gaudin, T.J., Giallombardo, A., Giannini, N.P., Goldberg, S.L., 2013. The placental mammal ancestor and the post-K-Pg radiation of placentals. Science 6120, 662–667.
Orliac, M.J., Ladevèze, S., Gingerich, P.D., Lebrun, R., Smith, T., 2014. Endocranial morphology of Paleocene *Plesiadapis tricuspidens* and the evolution of the early primate brain. Proc. R. Soc. B 281, 20132792.
Plavcan, J.M., 2000. Inferring social behavior from sexual dimorphism in the fossil record. J. Hum. Evol. 39, 327–344.
Plavcan, J.M., 2004. Evidence for early anthropoid social behavior. In: Ross, C.F., Kay, R.F. (Eds.), Anthropoid Origins: New Visions. Plenum Press, New York, pp. 383–413.
Radinsky, L.B., 1967. The oldest primate endocast. Am. J. Phys. Anthropol. 27, 385–388.
Radinsky, L.B., 1970. The fossil evidence of prosimian brain evolution. In: Noback, C.R., Motagna, W. (Eds.), The Primate Brain, Advances in Primatology, vol. 1. Appleton Century Crofts, New York, pp. 209–224.
Radinsky, L.B., 1974. Prosimian brain morphology: functional and phylogenetic implications. In: Martin, R.D., Doyle, G.A., Walker, A.C. (Eds.), Prosimian Biology. Duckworth, London, pp. 781–798.
Radinsky, L.B., 1975. Primate brain evolution. Am. Sci. 63, 656–663.
Radinsky, L.B., 1977. Early primate brains: facts and fiction. J. Hum. Evol. 6, 79–86.
Ramdarshan, A., Orliac, M., 2015. Endocranial morphology of *Microchoerus erinaceus* (Euprimates, Tarsiiformes) and early evolution of the euprimate brain. Am. J. Phys. Anthropol. 159, 5–16.
Rasmussen, D.T., 1987. Anthropoid origins: a possible solution to the Adapidae-Omomyidae paradox. J. Hum. Evol. 15, 1–12.
Rasmussen, D.T., 2007. Fossil record of the primates from the Paleocene to the Oligocene. In: Henke, W., Tattersall, I. (Eds.), Handbook of Paleoanthropology. Springer, Berlin, pp. 889–920.
Robinson, P., Gunnell, G.F., Walsh, S.L., Clyde, W.C., Storer, J.E., Stucky, R.K., Froehlich, D.J., Ferrusquia-Villafranca, I., McKenna, M.C., 2004. Wasatchian through Duschesnean biochronology. In: Woodburn, M.O. (Ed.), Late Cretaceous and Cenozoic Mammals of North America: Biostratigraphy and Geochronology. Columbia University Press, New York, pp. 106–155.
Rose, K.D., 1994. The earliest primates. Evol. Anthropol. 3, 159–173.
Rose, K.D., MacPhee, R.D.E., Alexander, J.P., 1999. Skull of early Eocene *Cantius adbitus* (Primates: Adapiformes) and its phylogenetic implications, with a reevaluation of "*Hesperolemur*" *actius*. Am. J. Phys. Anthropol. 109, 523–539.
Sauther, M.L., Cuozzo, F.P., 2012. Understanding Eocene primate paleobiology using a comprehensive analysis of living primate ecology, biology, and behaviour. Paleobio. Palaeoenv. 92, 573–583.
Schillaci, M.A., 2006. Sexual selection and the evolution of brain size in primates. PLoS One 1, e62.
Schillaci, M.A., 2008. Primate mating systems and the evolution of neocortex size. J. Mammol. 89, 58–63.
Seiffert, E.R., Perry, J.M., Simons, E.L., Boyer, D.M., 2009. Convergent evolution of anthropoid-like adaptations in Eocene adapiform primates. Nature 461, 1118–1122.
Schwartz, J.H., 1975. Re-evaluation of the morphocline of molar appearance in the primates. Folia Primatol. 23, 290–307.
Schmitt, D., 1996. Humeral head shape as an indicator of locomotor behavior in extant strepsirrhines and Eocene adapids. Folia Primatol. 67, 137–151.
Shultz, S., Dunbar, R., 2010. Encephalization is not a universal macroevolutionary phenomenon in mammals but is associated with sociality. Proc. Natl. Acad. Sci. 107, 21582–21586.
Silcox, M.T., Bloch, J.I., Boyer, D.M., Godinot, M., Ryan, T.M., Spoor, F., Walker, A., 2009a. Semicircular canal system in early primates. J. Hum. Evol. 56, 315–327.
Silcox, M.T., Dalmyn, C.K., Bloch, J.I., 2009b. Virtual endocast of *Ignacius graybullianus* (Paromyidae, Primates) and brain evolution in early primates. Proc. Natl. Acad. Sci. 106, 10987–10992.
Silcox, M.T., Benham, A.E., Bloch, J.I., 2010. Endocasts of *Microsyops* (Microsyopidae, Primates), and the evolution of the brain in primitive primates. J. Hum. Evol. 58, 505–521.
Simons, E.L., 1972. Primate Evolution: An Introduction to Man's Place in Nature. Plenum, New York.
Simons, E.L., Seiffert, E.R., Ryan, T.M., Attia, Y., 2007. A remarkable female cranium of the Oligocene anthropoid *Aegyptopithecus zeuxis* (Catarrhini, Propliopithecidae). Proc. Natl. Acad. Sci. 104, 8731–8736.
Smith, B.H., 1991. Age of weaning approximates emergence of the first permanent molar in non-human primates. Am. J. Phys. Anthropol. 12, 163–164.
Smith, B.H., Crummett, T.L., Brandt, K.L., 1994. Ages of eruption of primate teeth: a compendium for aging individuals and comparing life histories. Yearb. Phys. Anthropol. 37, 177–231.
Smith, R.J., 1993. Bias in equations used to estimate fossil primate body mass. J. Hum. Evol. 25, 31–41.
Smith, R.J., 2002. Estimation of body mass in paleontology. J. Hum. Evol. 43, 271–287.
Steiper, M.E., Seiffert, E.R., 2012. Evidence for a convergent slowdown in primate molecular rates and its implications for the timing of primate evolution. Proc. Natl. Acad. Sci. 6006–6011.
Stephan, H., Bauchot, R., Andy, O.J., 1970. Data on size of the brain and of various brain parts in insectivores and primates. In: Noback, C.R., Montagna, W. (Eds.), The Primate Brain. Appleton-Century Crofts, New York, pp. 289–297.
Szalay, F.S., 1969. Mixodectidae. Microsyopidae, and the insectivore-primate transition. Bull. Am. Mus. Nat. Hist. 140, 195–330.
Szalay, F.S., Delson, E., 1979. Evolutionary History of the Primates. Academic Press, New York.
Takai, M., Shigehara, N., Egi, N., Tsubamoto, T., 2003. Endocranial cast and morphology of the olfactory bulb of *Amphipithecus morgaungensis* (latest middle Eocene of Myanmar). Primates 44, 137–144.
Tattersall, I., Schwartz, J.H., 1974. Craniodental morphology and the systematics of the Malagasy lemurs (Primates, Prosimii). Anthropol. Pap. Am. Mus. Nat. Hist. 52, 139–192.
Wible, J.R., Covert, H.H., 1987. Primates: cladistic diagnosis and relationships. J. Hum. Evol. 16, 1–22.
Williams, B.A., Kay, R.F., Kirk, C.C., 2010a. New perspectives on anthropoid origins. Proc. Natl. Acad. Sci. 107, 4797–4804.
Williams, B.A., Kay, R.F., Kirk, E.C., Ross, C.F., 2010b. *Darwinius masillae* is a strepsirrhine—a reply to Franzen et al. (2009). J. Hum. Evol. 59, 567–573.
Winchester, J.M., Boyer, D.M., St Clair, E.M., Gosselin-Ildari, A.D., Cooke, S.B., Ledogar, J.A., 2014. Dental topography of platyrrhines and prosimians: convergence and contrasts. Am. J. Phys. Anthropol. 153, 29–44.
Yapuncich, G.S., Gladman, J.T., Boyer, D.M., 2015. Predicting euarchontan body mass: a comparison of tarsal and dental variables. Am. J. Phys. Anthropol. 157, 472–506.